

Using Similarity Distance Measures for Multiclass Damage Detection in Dynamically Monitored Structures

*Original*

Using Similarity Distance Measures for Multiclass Damage Detection in Dynamically Monitored Structures / Crocetti, A., Miraglia, G., Ceravolo, R.. - In: STRUCTURAL CONTROL & HEALTH MONITORING. - ISSN 1545-2255. - ELETTRONICO. - 2025:1(2025), pp. 1-20. [10.1155/stc/9593577]

*Availability:*

This version is available at: 11583/3004768 since: 2025-11-03T20:09:34Z

*Publisher:*

Wiley

*Published*

DOI:10.1155/stc/9593577

*Terms of use:*

This article is made available under terms and conditions as specified in the corresponding bibliographic description in the repository

*Publisher copyright*

(Article begins on next page)

## Research Article

# Using Similarity Distance Measures for Multiclass Damage Detection in Dynamically Monitored Structures

Alessio Crocetti <sup>1,2</sup> Gaetano Miraglia <sup>1,2</sup> and Rosario Ceravolo <sup>1,2</sup>

<sup>1</sup>Department of Structural, Geotechnical and Building Engineering, DISEG, Politecnico di Torino, Corso Duca Degli Abruzzi 24, Torino 10129, Italy

<sup>2</sup>Responsible Risk Resilience Interdepartmental Centre, R3C, Politecnico di Torino, Corso Duca Degli Abruzzi 24, Torino 10129, Italy

Correspondence should be addressed to Rosario Ceravolo; [rosario.ceravolo@polito.it](mailto:rosario.ceravolo@polito.it)

Received 23 December 2024; Revised 15 August 2025; Accepted 15 September 2025

Academic Editor: Jun Li

Copyright © 2025 Alessio Crocetti et al. Structural Control and Health Monitoring published by John Wiley & Sons Ltd. This is an open access article under the terms of the Creative Commons Attribution License, which permits use, distribution and reproduction in any medium, provided the original work is properly cited.

Domain adaptation (DA) techniques have recently been developed as a promising approach to enhance the performance of structural damage classification algorithms. Unlike traditional methods, DA imposes fewer constraints on the nature and completeness of datasets, although its effectiveness largely depends on the similarity between the datasets used for knowledge transfer. This paper proposes a novel approach for assessing structural similarity to improve DA in structural health monitoring (SHM). The identification of suitable source data for knowledge transfer in damage detection is an open issue in SHM, especially when dealing with important geometric, mechanical, and topological differences between the structures. To address this issue, damage detection accuracy is increased by investigating similarity in the modal features of different framed structures, with the aim of understanding their dynamic behavior through a similarity index based on divergence measures. In detail, this work proposes a novel modal sensitivity-based similarity index which relies on the Kullback–Leibler divergence computed from vibration-based dynamic features. This similarity index effectively reveals how structures differing in highly sensitive parameters exhibit greater divergence. When DA is applied, source datasets with higher similarity lead to improved multiclass damage classification accuracy on the target framed structure. The proposed index can be used to systematically rank candidate source structures before applying DA, allowing a more efficient selection process. Its applicability extends to large-scale structures, where managing heterogeneous structural datasets is essential, supporting data-driven SHM strategies with enhanced transferability and reliability in real-world monitoring scenarios.

**Keywords:** damage detection; domain adaptation; framed structures; similarity; structural health monitoring; vibration modes

## 1. Introduction

Farrar and Worden (2012) defined structural health monitoring (SHM) as a process that involves the periodic monitoring of a structure through measurements, the extraction of features symptomatic to the phenomena under investigation, and their statistical analysis to assess the current state of the system [1]. More specifically, in vibration-based SHM, modal parameters (e.g., natural frequencies and mode shapes) are critical indicators of structural characteristics such as stiffness and mass [2].

Data-driven approaches help in understanding the current structural condition by closely monitoring these features [3]. They exploit pattern recognition (PR), machine learning (ML), and other techniques aimed at producing a statistical representation of the system [4, 5]. This approach relies on algorithms and a large amount of data which can be retrieved directly from permanent or long-term monitoring systems to generate reliable statistics. The drawback of these methods, however, is that they do not provide a physically based interpretation of the input–output relationship, which limits their potential use (e.g., for prognosis evaluations). In

addition, the regression performed with these methods is often focus-based, making it difficult to accurately reproduce a wide range of behaviors. Typically, the structural state for which a large amount of data is available is associated with the undamaged condition. Both undamaged and damaged state data are required by ML algorithms to implement an efficient PR strategy. Damaged state data is rarely available in full-scale structures [6]. This may result in a lack of data in damaged conditions, which can pose an obstacle in the PR process.

In line with previous studies on structural damage detection during dynamic events [7–10], this work explicitly focuses on structural conditions sufficiently distant from strong motion or plasticization phases. Indeed, capturing reliable modal variations in proximity to such events requires instantaneous estimators, for instance recurring to time-frequency analyses or adaptive techniques. This positioning reflects the intended applicability of the method to quasistationary regimes, while explicitly recognizing that transient, nonstationary effects require specialized analyses beyond the current scope.

Transfer learning (TL), and in particular domain adaptation (DA) [11], can be considered a valuable tool for addressing the issue of data scarcity. It is embedded in ML technologies and allows the use of training datasets from one or more systems in order to initialize an algorithm, without the need for sharing the same distributions or tasks [12–15]. This technology is used to transfer information from a more informed system (source) to another system (target) characterized by a lack of information, for example, due to a small number of available data, while sharing some properties with the source. DA is a TL technique that explicitly focuses on aligning source and target domains with different distributions [16], without requiring fine-tuning, which is often necessary when deep neural networks are used [17–20].

Selecting the correct source system is fundamental. In this regard, the concept of similarity offers a powerful tool for comparing structural behavior. Similarity involves examining the intrinsic characteristics common to objects, such as their structures or attributes, to make them suitable for quantitative comparison.

In the SHM field, the concept of similarity is used in the *population-based structural health monitoring (PBSHM)* approach [21], which considers groups of structures to enhance the knowledge used to predict damage conditions, making use of techniques such as DA. Similarity in structures can be assessed based on physical properties of the structure (such as geometry, material, and topology), and it stands as a key factor in DA outcomes. On the other hand, when considering similarity within data domains (e.g., features), it is crucial to introduce the concept of distance, which represents the degree of separation between two objects. Distances are divided into metrics and divergences. The choice of an appropriate distance measure is fundamental when dealing with assessing similarity between domains, as it directly influences the correct diagnosis of the structural state of a system. A detailed discussion of the properties and implications of these distances, with a focus on divergences, will be provided in Section 2.

Similarity between domains must be carefully explored to avoid the concept of *negative transfer*, when the performance of the algorithm on the target system turns out to be worsened by the transfer of source datasets, yielding better results when trained only on the target data for classification tasks.

*1.1. Research Significance.* This study focuses on divergence-based approaches to assess the similarity of modal distribution data by means of the Kullback–Leibler divergence, a nonsymmetric measure used to assess the difference between two probability distributions over the same variable [22]. The proposed methodology aims to assist in selecting an appropriate source structure for DA through transfer component analysis (TCA) in multiclass damage detection scenarios. Specifically, a similarity index based on the normalized Kullback–Leibler divergence is introduced as a novel tool for future DA applications that leverage modal features. This novel approach provides valuable insights into the field of SHM, enabling the identification, in advance, of the most suitable monitored structure to be used as *source structure* when DA techniques are applied to sparsely monitored target structures.

This paper focuses on numerical models of a three-story aluminum frame, developed to generate reliable datasets representing both damaged and healthy conditions. Additionally, three distinct groups of heterogeneous three-story structures were selected, each characterized by variations in geometric and mechanical parameters that significantly influence their modal behavior (e.g., natural frequencies and mode shapes). To optimize the selection of source structures groups, a local sensitivity analysis was performed by evaluating the modal similarity between each source structure and the target structure. Finally, a multiclass classification problem for damage detection in the target frame is compared with the DA classification results obtained using the selected source group. This comparison allows for the determination of a modal similarity index, which is directly linked to the effectiveness of the DA application.

The article is organized as follows: Section 2 introduces the concept of structural similarity between data distributions, highlighting its relevance in data-driven SHM and DA approaches. Section 3 provides an overview of the DA techniques and algorithms used in the analysis. Section 4 describes the application of an aluminum frame, focusing on three distinct sets of heterogeneous source structures for which noisy modal datasets are generated. Section 5 presents a similarity index based on the Kullback–Leibler divergence theory. Section 6 outlines the expansion of damage data using neural network surrogate models, generating datasets to perform DA through TCA for each structural group. This section also evaluates the relationship between the Kullback–Leibler divergence and TCA accuracy. Finally, a numerical study examines the impact of vibration mode similarity on TCA results, providing a generalized understanding of the concept. In Section 7, the conclusions of the study are drawn.

## 2. The Concept of Similarity

**2.1. Theoretical Background on Similarity.** In broad terms, similarity can be described by analyzing the inherent features shared by objects (e.g., structures), which make them quantitatively comparable. In the case of structures, similarity can be evaluated based on their physical attributes or by examining their mechanical features, such as modal parameters. These properties often serve as primary datasets for data-driven methodologies, including ML and, more specifically, TL. Indeed, structural similarity is intrinsically linked to similarities in the data and vice versa. Gardner et al. [23] defined the physical properties within a population of structures as comprising geometry, material, and topology. The first includes the shape, size, and scaling of a structure, while the second pertains to the material properties that define its structural elements. The third concept addresses various topological features of the structure as a whole, such as boundary conditions and multibody relationships. In a recent work, Wickramarachchi et al. [24] focused on using distance-based measures to assess similarity in order to gain insights into a population lacking prior knowledge, with the purpose of supporting DA in PBSHM.

When assessing similarity through data domains, it is important to introduce the concept of *distance*, which refers to the extent of farness between two objects. When these distances adhere to metric quantities, they are referred to as *metrics*, while other nonmetric quantities are known as *divergences* [25]. In stochastic data, probability density functions (PDFs) are often used. Vector and probabilistic approaches are commonly used to assess PDF distance/similarity measures. The first treats each PDF as a vector, and various geometric distances are used to compare them. In particular, discrete versions of several divergences are often used [26]. On the other hand, the probabilistic method relies on the premise that a histogram of a measurement serves as the foundation for an empirical approximation of the PDF. The Ali–Silvey distance [27], also known as Csiszar’s  $\phi$ -divergence [28], stands as a prominent member within the extensively examined and deeply understood families of distances/divergences between probability measures [29]. This metric is defined as

$$D_{\phi}(\mathbb{P}, \mathbb{Q}) := \begin{cases} \int_M \phi\left(\frac{d\mathbb{P}}{d\mathbb{Q}}\right) d\mathbb{Q}, & \mathbb{P} \ll \mathbb{Q}, \\ +\infty, & \text{otherwise,} \end{cases} \quad (1)$$

with  $M$  representing a measurable space and  $\phi$  a convex function.  $\mathbb{P} \ll \mathbb{Q}$  indicates that  $\mathbb{P}$  is absolutely continuous with respect to  $\mathbb{Q}$ . By properly choosing  $\phi$ , different kinds of distance/divergence measures are determined (Table 1), among numerous other options [30, 31].

In 2009, Sriperumbudur et al. [32] examined the relationships among metrics based on PDFs, specifically  $\phi$ -divergences and integral probability metrics (IPM) and introduced several innovative characteristics to enhance their practical usability. Synthetically, the IPMs [33] are defined as

TABLE 1: Distance and divergence measures among the Csiszar’s  $\phi$ -divergence family.

Measure	$\phi(t)$
Kullback–Leibler divergence	$t \log(t)$
Hellinger distance	$(\sqrt{t} - 1)^2$
Variation distance	$ t - 1 $
$\chi^2$ -Divergence	$(t - 1)^2$

$$\gamma_{\mathcal{F}}(\mathbb{P}, \mathbb{Q}) := \sup_{f \in \mathcal{F}} \left| \int_M f d\mathbb{P} - \int_M f d\mathbb{Q} \right|, \quad (2)$$

where  $\mathcal{F}$  is a real-valued bounded class measurable function on  $M$ .

Another approach to assess similarity relies on indicators. One of them, the Modal Assurance Criterion (MAC), is a statistical operator used to measure the consistency (degree of linearity) between different estimates of a modal vector [34]. One application of MAC is the evaluation of similarity through mode shapes comparison. Hughes et al. [35] assessed structural similarity in a physics-informed way by providing a modal shapes similarity score via MAC as a predictor of DA quality. Recently, Bunce et al. [36] employed MAC to assess similarity between the mode shapes from a set of bridges in the context of PBSHM.

**2.2. Similarity in Data-Driven Approaches to Damage Detection.** Due to the absence of sufficient monitoring data, DA is increasingly used in SHM. This makes the analysis of data domains crucial for transferring information from *source* to *target* systems. Here, a question arises: is structural (topological, geometric, and mechanical) similarity fully correlated with modal data similarity? The question is important because damage detection is often performed using data from modal parameters rather than from geometric and mechanical properties (hereafter referred to as properties), with DA classification performance following the same concept. Bull et al. [21] addressed the concept of PBSHM, which aims to share information from one group of structures within a population to another, with the goal of improving damage detection predictions for each member of the population. The study focused on populations of shear structures which differed in both topology and label space. A population can be either *homogeneous* or *heterogeneous* [37]. It is considered homogeneous if any pair of structures within the population is nominally identical. In contrast, a set of different (nonidentical) structures belongs to a heterogeneous population. This distinction clearly reflects the level of similarity between structures: various parameters lead to a different level of heterogeneity, depending on the framework. Gosliga et al. [37] described the concepts of irreducible element (IE) models and attributed graphs (AGs) metrics to characterize structural attributes. In their study, Delo et al. [38] expanded on this concept, focusing on the mechanical and geometric differences in distance metrics within a heterogeneous population of laboratory-scale aircraft case study, ending reproducing a graph matching network (GMN) to evaluate a similarity matrix.

Dissimilarities in data are not always consistent within a set of structures. Data acquisition and processing can significantly affect features: even when considering a pair of structures with homogeneous physical properties, data heterogeneity can be observed. Therefore, dissimilarity must be taken into account when DA is conducted. For instance, sensor placement can influence this effect, leading to differences in the data when processed.

This study aims to define a modal similarity index in the context of heterogeneous framed structures with a consistent label space, using the Kullback-Leibler ( $D_{KL}$ ) divergence [22]. Consistency of label space is ensured when features belonging to one system (i.e., structure) have the same dimension as those from the other system, which serves as the target. In this paper, the number of natural frequencies, mode shapes, and eigenvectors, as well as the labels corresponding to different damage typologies for multiclass classification, are the same.

Modal similarity is compared with physical similarity: structures with different properties are linked to their modal data distribution. According to the target structure under investigation, some parameters will prove more important than others in the DA multiclass damage detection due to their impact on modal behavior.

### 3. Description of DA Algorithms

**3.1. DA Techniques.** In the SHM framework, the data used to train ML algorithms often come from the same distributions, meaning that both the structures and the acquisition time periods are identical. This results in homogeneous datasets obtained from measurements, which can be processed by the specific algorithm.

This is not always feasible, particularly due to the lack of data in damaged conditions or their overall scarcity. Gardner et al. [11] applied the TCA algorithm in various applications, comparing its performance with other DA techniques, namely, joint domain adaption (JDA) and adaptation regularization-based transfer learning (ARTL). Tronci et al. [39] utilized an extensive acoustic dataset to gain experience in damage classification, applying it to simulated data from a 12 degrees of freedom (DoFs) benchmark shear-building structure. Coletta et al. [3] addressed the challenge of the lack of labeled data related to different structural conditions of a monumental building by employing TCA.

Additionally, virtual data generated through FE models were utilized to train ML algorithms and support the interpretation of real measurements. Cavanni et al. [40] exploited kernelized Bayesian transfer learning (KBTL) [41] to improve classification accuracy for monitoring historical buildings.

This paper presents a DA application (Figure 1) aimed at enhancing the accuracy of a support vector machine (SVM) classifier in detecting damage on a little-known structure (target) through a DA algorithm, specifically the TCA. Poole et al. [42] compared TCA with statistical alignment (SA) algorithms across three different case studies: (i) a heterogeneous numerical population of three-story structures, (ii) a real heterogeneous population consisting of two bridges,

the Z24 [43] and the KW51 [44], and (iii) an analysis of the use of SA as a preprocessing method to simplify the DA problem has been conducted. Giglioni et al. [45] introduced a novel framework for damage classification in bridge monitoring, utilizing DA techniques to align and transform (SA) natural frequencies (features sensitive to damage) into a common feature space. Gardner et al. [46] proposed DA techniques to address data distribution shifts caused by structural repairs in SHM. The metric-informed joint distribution adaptation (M-JDA) method outperformed other DA techniques, demonstrating its potential to enhance the industrial applicability of data-driven SHM.

DA is a subcategory of TL methods that focuses on transferring knowledge between two systems that are related in some way, by exploiting their associated data domains [13, 47]. The term *domain* can be explained through two distinct components:

- Feature space of input  $\mathcal{X}$ ;
- Marginal distribution  $P(\mathbf{X})$  of a set of inputs  $\mathbf{X} = \{\mathbf{x}_1, \dots, \mathbf{x}_n\}^T \in \mathcal{X}$ .

Considering the different systems, two domains can be defined according to DA: a source domain  $\mathcal{D}_S$  and a target domain  $\mathcal{D}_T$ . A task is represented by  $\mathcal{T} = \{\mathcal{Y}; f(\cdot)\}$ , which can be assigned to each domain, where  $\mathcal{Y}$  denotes the label space and  $f(\cdot)$  represents the objective predictive function used to predict the corresponding label. A common way to define the latter is  $P(y|x)$ . The labeled data are contained in  $\mathcal{D}_S$  (equation (3)) and they represent the information that needs to be transferred. It can be analytically defined as

$$\mathcal{D}_S = \left\{ (\mathbf{x}_{S,1}, y_{S,1}), \dots, (\mathbf{x}_{S,n_S}, y_{S,n_S}) \right\}^T. \quad (3)$$

The data from the target system are contained in  $\mathcal{D}_T$  (equation (4)) and they can be either unlabeled or only partially labeled:

$$\mathcal{D}_T = \left\{ (\mathbf{x}_{T,1}, y_{T,1}), \dots, (\mathbf{x}_{T,n_T}, y_{T,n_T}) \right\}^T, \quad (4)$$

where  $\mathbf{x}_{S,i} \in \mathcal{X}_S$  represent the  $n_s$  observations and the corresponding output  $y_{S,i} \in \mathcal{Y}_S$  can be interpreted as the structural conditions in the case of SHM. On the other hand,  $\mathbf{x}_{T,i} \in \mathcal{X}_T$  represent the  $n_T$  observations in the target domain, which can be either unlabeled or partially labeled, and  $y_{T,i} \in \mathcal{Y}_T$  may or may not be available for each feature observation  $\mathbf{x}_{T,i} \in \mathcal{X}_T$ .

Feature and label spaces can be considered to be identical for both source and target domains in DA methods, that is,  $\mathcal{X}_S = \mathcal{X}_T$  and  $\mathcal{Y}_S = \mathcal{Y}_T$ . In the SHM field, this implies that both systems share the same diagnostic properties and the structural conditions. Actually, the systems differ in their marginal distributions and, in some cases, in their conditional distributions as well. This leads to diagnostic features being distributed differently,  $P(\mathbf{X}_S) \neq P(\mathbf{X}_T)$ , and reflects the differences in the probabilities associated with the occurrence of structural conditions (labels),  $P(\mathbf{Y}_S|\mathbf{X}_S) \neq P(\mathbf{Y}_T|\mathbf{X}_T)$ , as these features exhibit dissimilarities between the source and the target domains. Due to these differences,

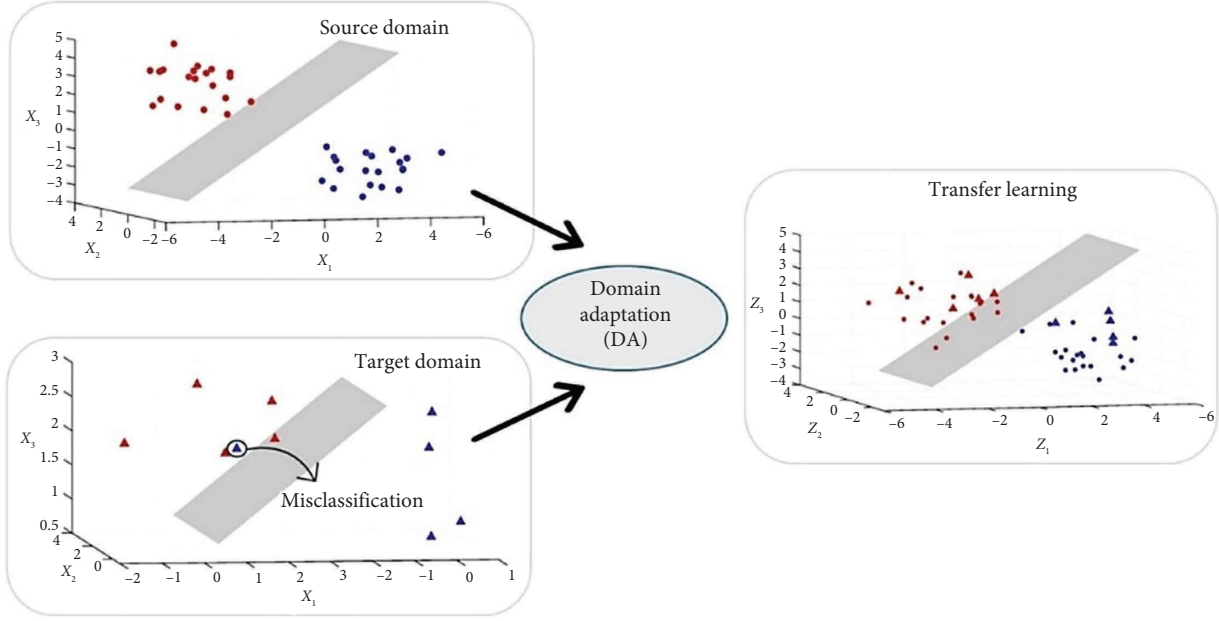


FIGURE 1: The figure illustrates the process of DA. On the left, the classification results for the source and target domains are reported. On the right, the misclassification error of the original target domain is addressed through DA.

training a classifier on the source domain and directly testing it on the target domain may mislead the algorithm.

To address this issue, several methods have been introduced to reduce the distance between the source and target domain distributions. These techniques employ a nonlinear mapping function  $\phi(\cdot)$ , which aligns the distributions, ensuring  $P(\phi(\mathbf{X}_S)) \approx P(\phi(\mathbf{X}_T))$  and  $P(\mathbf{Y}_S|\phi(\mathbf{X}_S)) \approx P(\mathbf{Y}_T|\phi(\mathbf{X}_T))$ . In this paper, TCA [47], a novel developed learning algorithm, has been employed to reduce the distance between data distributions.

**3.1.1.1. TCA.** TCA [47] aims at finding the mapping function  $\phi(\cdot)$  from the source space to a reproducing kernel Hilbert space (RKHS) using as embedded criterion the maximum mean discrepancy (MMD), minimizing the distance between the marginal probabilities  $P(\phi(\mathbf{X}_S))$  and  $P(\phi(\mathbf{X}_T))$  and keeping  $P(\mathbf{Y}_S|\phi(\mathbf{X}_S)) \approx P(\mathbf{Y}_T|\phi(\mathbf{X}_T))$ .

The function  $\phi$  can be found as feature map determined by a universal kernel. The MMD distance between the two different data distributions may be measured through the distance (equation (5)) between the empirical means of the source and target domains as follows:

$$\text{Dist}(\mathbf{X}'_S, \mathbf{X}'_T) = \text{tr}(\mathbf{KL}), \quad (5)$$

where  $\mathbf{X}'$  represent the transformed inputs from the original domains,  $\mathbf{K} = k(\mathbf{X}, \mathbf{X}') \in \mathbb{R}^{(n_S+n_T) \times (n_S+n_T)}$  is associated to the Kernel matrix, where  $\mathbf{X} = \{\mathbf{X}_S, \mathbf{X}_T\}^T$  and  $\mathbf{L}$  (equation (6)) is the MMD matrix, defined as

$$\mathbf{L}(i, j) = \begin{cases} \frac{1}{n_S^2}, & \text{if } \mathbf{x}_i, \mathbf{x}_j \in \mathbf{X}_S, \\ \frac{1}{n_T^2}, & \text{if } \mathbf{x}_i, \mathbf{x}_j \in \mathbf{X}_T, \\ -\frac{1}{n_S n_T}, & \text{otherwise.} \end{cases} \quad (6)$$

By exploiting a weight matrix  $\mathbf{W} \in \mathbb{R}^{(n_S+n_T) \times m}$ , through a kernel matrix decomposition, the empirical kernel map becomes  $\tilde{\mathbf{K}} = \mathbf{K}\mathbf{W}\mathbf{W}^T\mathbf{K}$  [48], reducing the feature vector in a space defined by  $m$  dimensions. By replacing  $\tilde{\mathbf{K}}$ , the above distance can be defined as

$$\text{Dist}(\mathbf{X}'_S, \mathbf{X}'_T) = \text{tr}(\mathbf{W}^T\mathbf{K}\mathbf{L}\mathbf{K}\mathbf{W}). \quad (7)$$

A regularization term is introduced in the distance minimization to control  $\mathbf{W}$ , rewriting the kernel problem to avoid the trivial solution  $\mathbf{W} = 0$ , introducing the constraints

$$\begin{aligned} \min_{\mathbf{W}} \text{tr}(\mathbf{W}^T\mathbf{K}\mathbf{L}\mathbf{K}\mathbf{W}) + \mu \text{tr}(\mathbf{W}^T\mathbf{W}), \\ \text{s.t. } \mathbf{W}^T\mathbf{K}\mathbf{L}\mathbf{K}\mathbf{W} = \mathbf{I}_m, \end{aligned} \quad (8)$$

where  $\mu > 0$  is a regularization/trade-off parameter,  $\mathbf{H} = \mathbf{I}_{n_S+n_T} - 1/(n_S + n_T)\mathbf{1}\mathbf{1}^T$  (see [47]) is the centering matrix, with  $\mathbf{I}_{n_S+n_T} \in \mathbb{R}^{(n_S+n_T) \times (n_S+n_T)}$  representing the identity matrix, and  $\mathbf{1} \in \mathbb{R}^{n_S+n_T}$  is the column vector with all ones.

Hence,  $\mathbf{I}_m \in \mathbb{R}^{m \times m}$  represents the identity matrix (where  $m \leq n_S + n_T - 1$ ) and  $\mathbf{W}^T \mathbf{K} \mathbf{H} \mathbf{K} \mathbf{W}$  corresponds to the variance of the projected samples needed to be preserved in TCA. To simplify notation, it will be omitted the subscript  $m$  from  $\mathbf{I}_m$  in the following. Using a Lagrangian approach, the optimization problem which involves a nonconvex norm constraint  $\mathbf{W}^T \mathbf{K} \mathbf{H} \mathbf{K} \mathbf{W} = \mathbf{I}$ , equation (8) can be solved by optimizing the equivalent trace problem in equation (9), as shown in the following [47]:

$$\max_{\mathbf{W}} \text{tr} \left( \left( \mathbf{W}^T (\mathbf{K} \mathbf{L} \mathbf{K} + \mu \mathbf{I}) \mathbf{W} \right)^{-1} \mathbf{W}^T \mathbf{K} \mathbf{H} \mathbf{K} \mathbf{W} \right), \quad (9)$$

where  $\mathbf{W}$  can be solved by deriving the  $m$  leading eigenvectors of  $(\mathbf{K} \mathbf{L} \mathbf{K} + \mu \mathbf{I})^{-1} \mathbf{K} \mathbf{H} \mathbf{K}$ , where  $m \leq n_S + n_T - 1$ , that describe the space of the transformed feature by means of  $\mathbf{Z} = \mathbf{K} \mathbf{W} \in \mathbb{R}^{(n_S + n_T) \times m}$ .

Finally, to evaluate the performance of the algorithm used in the classification process, a metric is defined based on the number of True Positives (TP), False Positives (FP), True Negatives (TN), and False Negatives (FN):

$$\text{Accuracy} = \frac{\text{TP} + \text{TN}}{\text{TP} + \text{TN} + \text{FP} + \text{FN}}. \quad (10)$$

## 4. Modal Sensitivity Analysis for Similarity Assessment

**4.1. Benchmark Structure.** The benchmark structure used in this study is an aluminum frame built in the Laboratory of Earthquake Engineering and Dynamics (EED Laboratory) at the Polytechnic of Turin (Figure 2). The structure is a three-story frame with a square plan, 0.4 m in width, and a total height of 0.9 m. Four columns support the structure and they are fixed at the base end to a steel plate which acts as a foundation plate. Most of the structural elements, constituted by columns and slabs, are made of aluminum. The slabs are constituted of square plate elements, whose thickness is 5 mm, and the floor decks are considered rigid in their plane. Diaphragmatic floor behavior is assumed for the structure. The columns, such as the diagonal bracings, are characterized by rectangular sections  $20 \times 3$  mm. Columns and slabs are joined using galvanized steel L-profiles that measure  $20 \times 20$  mm with a thickness of 2 mm. The connections between the columns and the ground are made using the same components but with dimensions of  $30 \times 30$  mm. Braces consist of ties pinned at the end nodes, while the other connections, including the beam-slab ones, can be assumed as rigid.

The mechanical properties of the aluminum structural elements are defined by a Young's modulus of 69,000 MPa, a Poisson's ratio of 0.326, and a density of  $2700 \text{ kg/m}^3$ . A simplified numerical model has been developed to apply damage to the structure and evaluate its modal behavior (Figure 3(a)), that is, by altering the values of natural frequencies for each damage scenario. In particular, the model has nine DoFs, six in the horizontal plane and three rotations about the vertical axis. The numerical structure is assumed to have 144 observations under the same structural condition,

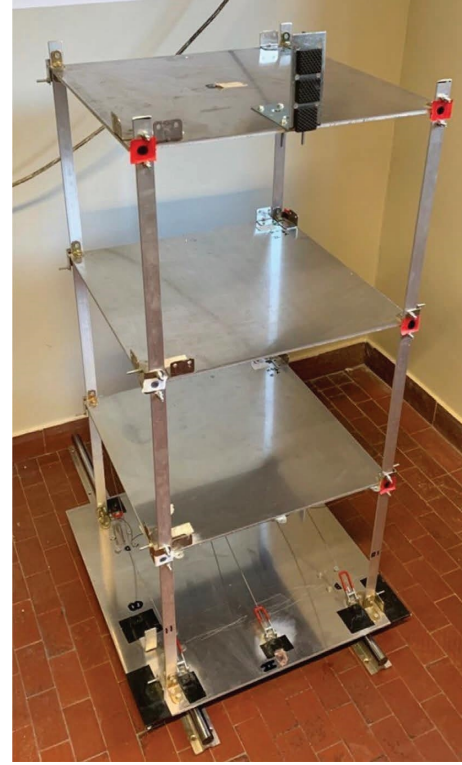


FIGURE 2: Three-story aluminum structure built in the laboratory of earthquake engineering and dynamics at the Polytechnic of Turin.

corresponding to the experimental observations collected in a single day for the benchmark frame. In this study, the numerical model of the benchmark structure, with fixed geometric, mechanical, and topological characteristics, is considered as target system. Figure 3(b) shows the nomenclature associated with the elements of the numerical model.

**4.2. Sensitivity Analyses on Vibration Modes.** The proposed method involves performing eigenvalue analysis to determine the modal features of the benchmark frame and categorizing source datasets for DA based on similar modal behavior. This is achieved by generating different groups of structures with the same topology as the benchmark, but varying parameters.

To evaluate the effects of parameter variation on modal behavior in terms of natural frequencies, local sensitivity analyses [49] of the properties related to the numerical model (target system) are conducted hereinafter. The model consists of structural components with uniform material characteristics. In this study, within the linear elastic field, which considers three material properties for each component (i.e., Young's modulus  $E$ , Poisson ratio  $\nu$ , and material density  $\rho$ ), the sensitivity analysis examines variations in only two of these properties: Young's modulus  $E$  and material density  $\rho$ . Regarding the geometric properties of the structural components, the height and the depth of the sections of each column, as well as the bracing area, are considered as variables in the analysis. In this context, the

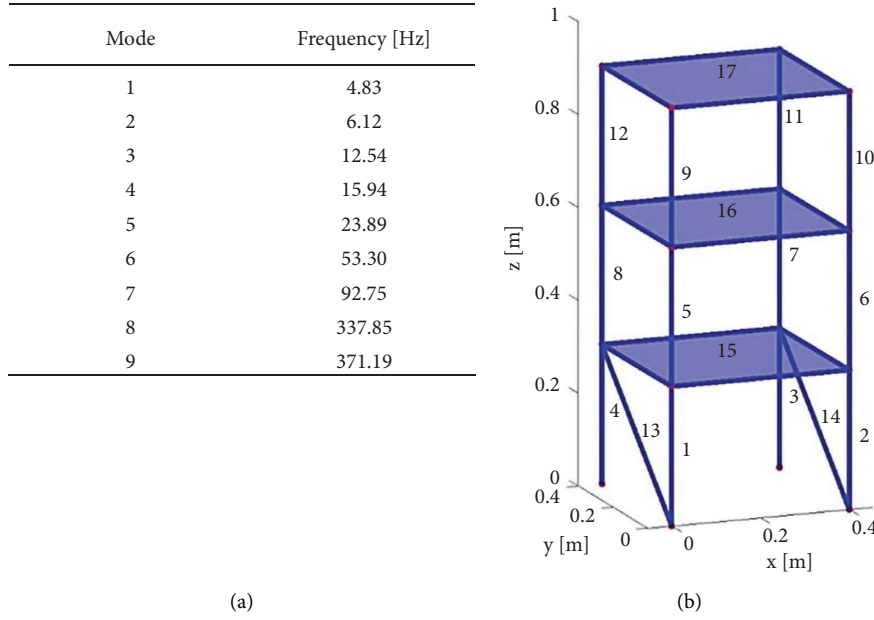


FIGURE 3: Natural frequencies of the three-story aluminum frame, along with the corresponding mode shapes identified through the numerical model (a). Element identification labels for the benchmark numerical structure (target) (b).

coefficients of variation (CV) for the first three natural frequencies associated with the  $i$ -th parameter of the target system have been computed.

The CV is then scaled with respect to the values of the involved parameters. The scaled  $CV_{i,scaled}$  (equation (11)) for the corresponding vibrational modes effect of the  $i$ -th parameter is

$$CV_{i,scaled} = \frac{CV_{i,f}}{CV_{i,p}} CV_{i,p_{real}}, \quad (11)$$

where  $CV_{i,f}$  represents the coefficient of variation of the frequencies,  $CV_{i,p}$  denotes the coefficient of variation of the  $i$ -th parameter, and  $CV_{i,p_{real}}$  refers to the chosen boundary variations (i.e., realistic damages) according to the system. Once the  $CV_{i,scaled}$  has been computed for each parameter, it is possible to determine the contribution of each coefficient of variation ( $CV_{i,scaled,\%}$ ) (equation (12)) to the sum of all contributions as follows:

$$CV_{i,scaled,\%} = 100 \frac{CV_{i,scaled}}{\sum_j CV_{j,scaled}}, \quad (12)$$

with  $j$  taking values between 1 and the total number of parameters considered in the analysis. The higher the  $CV_{i,scaled,\%}$  of the  $i$ -th parameter, the greater the impact its variation will have on the natural frequency content of the target structure.

In this study, two different sensitivity analyses are conducted: (i) the first is used to create three Groups of Structures (GoS),  $GP_S$ , where  $S$  is a free variable taking values between 1 and 3, corresponding to the selected group of 21 out of 63 varying parameters, based on the percentage contribution of the coefficient of variation in descending order. These three-story frames will be used as numerical

source structures for DA purposes. (ii) The second sensitivity analysis is performed to introduce three different types of damage by varying the values of elastic parameters, each belonging to a specific GoS. The scaled CV described in equation (11) can only be applied to the second analysis, as it allows defining the range of variation for the properties. For example, the crack length can vary between zero and the depth of the section.

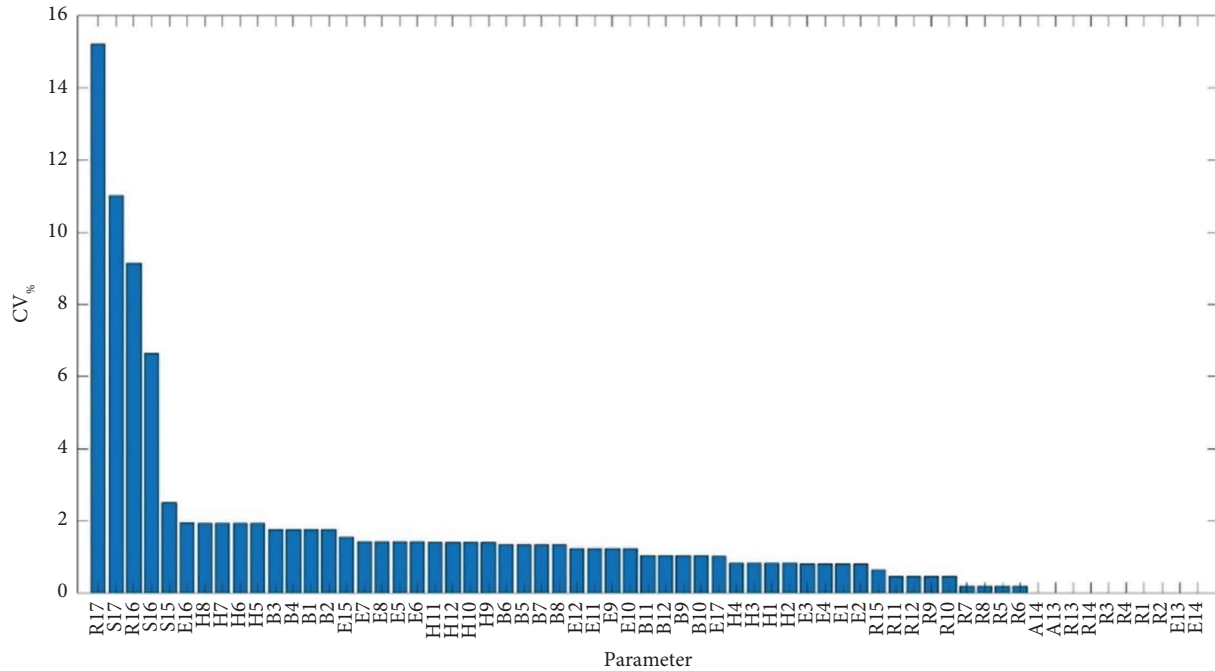
**4.2.1. Modal Similarity Analysis for Source Framed Structures.** To obtain source structures that vary geometrically and mechanically from the target structure, a similarity analysis is conducted to identify three different GoS. These GoS share common same varying parameters (Young's modulus  $E$ , material density  $\rho$ , base  $b$ , height  $h$ , and thickness  $s$ ), which are selected based on their similar modal effects on the target structure. The sensitivity analysis is then performed by varying these properties one at a time, between a maximum and a minimum value (Table 2). The first three natural frequencies are selected and their  $CV_{i,f}$  values are derived. In addition, the  $CV_{i,\%}$  are evaluated (Figure 4).

$$CV_{i,\%} = 100 \frac{CV_{i,f}}{\sum_j CV_{j,f}}. \quad (13)$$

Based on the  $CV_{i,\%}$ , the parameters are divided into three distinct groups, each containing 21 parameters, both geometric and mechanical. The first group includes the 21 parameters with the highest  $CV_{i,\%}$ , representing the most modal sensitive group. The second group contains the 21 parameters located in the middle of the  $CV_{i,\%}$  plot, while the third and final group includes the 21 parameters with the lowest  $CV_{i,\%}$ , making them the least sensitive to modal variations (Table 3). These groups will define three distinct

TABLE 2: Nominal, maximum, and minimum values of properties related to the target structure for sensitivity analysis purposes.

Parameter	Symbol	Nominal value	Maximum value	Minimum value
$E$ (Pa)	E	6.90E + 10	6.90E + 11	6.90E + 09
$\rho$ (kg/m <sup>3</sup> )	R	2.70E + 03	2.70E + 04	2.70E + 02
$b$ (m)	B	2.00E - 02	2.00E - 01	2.00E - 03
$h$ (m)	H	3.00E - 03	3.00E - 02	3.00E - 04
$A$ (m <sup>2</sup> )	A	6.00E - 05	6.00E - 04	6.00E - 06
$s$ (m)	S	5.00E - 03	5.00E - 02	5.00E - 04

FIGURE 4: Coefficients of variation ( $CV_{\%}$ ) of parameters for the sensitivity analysis aimed at selecting the Group of source Structures (GoS). The parameters are described with their symbols (Table 2) and corresponding elements (Figure 3(b)).

sets of source structures, each sharing a similar modal behavior.

**4.2.2. Sensitivity of Vibration Modes for Damage Detection.** Here, the sensitivity analysis aims to select the damage to be introduced in the structures. The ranges for the parameters of the target structure that are subjected to variation are described in Table 4. Finally, the  $CV_{i,scaled,\%}$  have been computed (Figure 5). According to Table 5, damages are simulated by varying three parameters each belonging to a different GoS, which is characterized by a similar behavior (Table 3).

As acknowledged in recent literature, variations in modal parameters can arise from Environmental and Operational Variations (EOVs) or other random and nonlinear structural behaviors and may not necessarily indicate the presence of damage. This phenomenon is particularly relevant in vibration-based SHM, where distinguishing true damage effects from operationally induced variability remains an open challenge [50, 51]. For instance, highly nonlinear and hysteretic behaviors, often manifested as “frequency wandering” during earthquake swarms or temperature-induced stiffness variations, can cause apparent

shifts in modal frequencies. A clear example is presented in the work [52], which proposes a method to define damage thresholds based on statistical modeling of modal parameter variations, explicitly addressing the minimization of false alarms in SHM systems. In the study, the authors highlight the need to consider the dispersion of modal features due to EOVs when defining decision boundaries for damage detection. The authors use a probabilistic approach to determine adaptive thresholds that account for the natural variability of modal features, improving the reliability of classification between damaged and undamaged states. Therefore, in this study, the influence of EOVs on modal features has been simulated by perturbing the mechanical parameters associated with the structural model (see Table 6).

**4.3. Generation of Vibration Mode Datasets: Source Structures.** Different source structures can be numerically modeled by varying the properties associated with a single GoS, while keeping all other parameters constant relative to the target fixed values. Thus, with reference to the parameters listed in Table 3, the Latin Hypercube Sampling (LHS) method [53–55] is used for statistically sampling parameter values,

TABLE 3: Parameters related to the properties of each group of structures (GoS),  $GP_s$ .

GP	Parameter																				
1	R17	S17	R16	S16	S15	E16	H8	H7	H6	H5	B3	B4	B1	B2	E15	E7	E8	E5	E6	H11	H12
2	H10	H9	B6	B5	B7	B8	E12	E11	E9	E10	B11	B12	B9	B10	E17	H4	H3	H1	H2	E3	E4
3	E1	E2	R15	R11	R12	R9	R10	R7	R8	R5	R6	A14	A13	R13	R14	R3	R4	R1	R2	E13	E14

TABLE 4: Nominal, maximum, and minimum (scaled) values of properties related to the target structure for sensitivity analysis purposes (damages).

Parameter	Nominal value	Maximum value	Minimum value	Minimum value (scaled)
$E$ (Pa)	$6.90E + 10$	$6.90E + 10$	$4.83E + 10$	$6.00E + 10$
$\rho$ ( $kg/m^3$ )	$2.70E + 03$	$2.70E + 03$	$2.20E + 03$	$2.40E + 03$
$b$ (m)	$2.00E - 02$	$2.00E - 02$	$2.00E - 03$	$1.97E - 02$
$h$ (m)	$3.00E - 03$	$3.00E - 03$	$3.00E - 04$	$2.80E - 03$
$A$ ( $m^2$ )	$6.00E - 05$	$6.00E - 05$	$6.00E - 06$	$5.52E - 05$
$s$ (m)	$5.00E - 03$	$5.00E - 03$	$5.00E - 04$	$4.70E - 03$

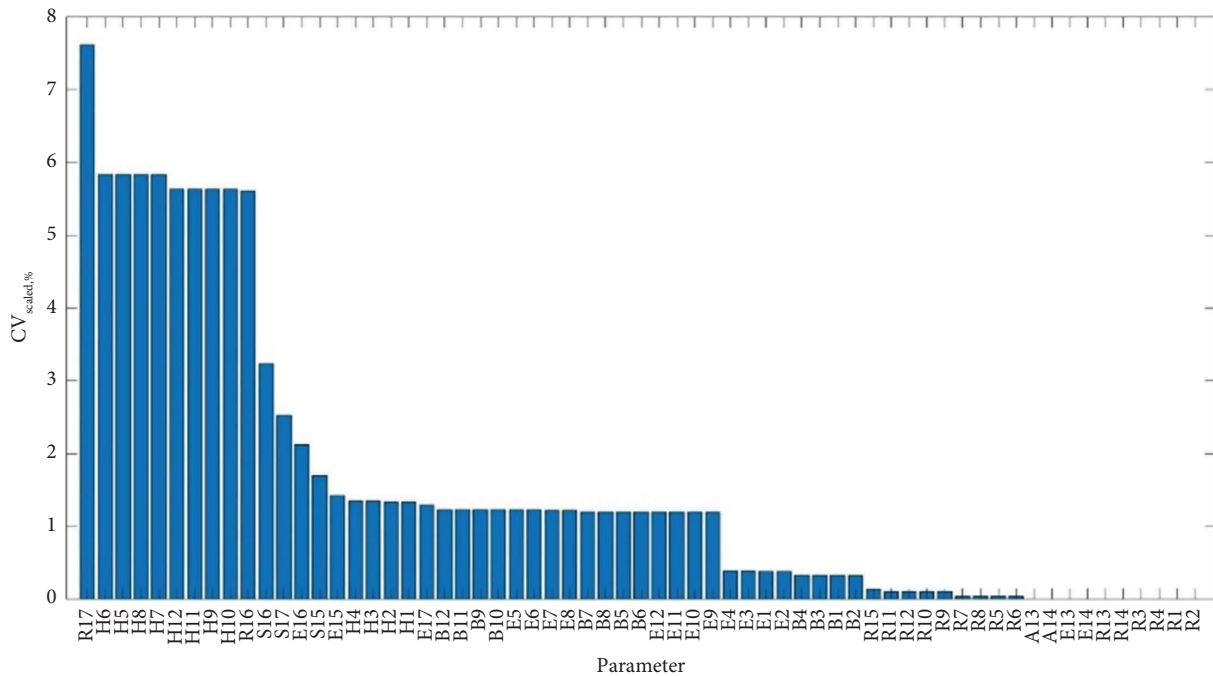


FIGURE 5: Coefficients of variation ( $CV_{scaled, \%}$ ) of parameters for the sensitivity analysis aimed at identifying damages to be introduced in the properties. The parameters are described with their symbols (Table 2) and corresponding elements (Figure 3(b)).

TABLE 5: Damages introduced for each parameter and their respective nomenclature.

Parameter	Nomenclature	Damage ID
$\rho$ ( $kg/m^3$ )	R17	1
$h$ (m)	H10	2
$A$ ( $m^2$ )	A14	3

TABLE 6: Observational variability in parameters belonging to each Group of Structures (GoS),  $GP_s$ , where S ranges from 1 to 3.

GP	Parameter		Range of variation	
1	R17	E16	-33%	+33%
2	E12	E11	-33%	+33%
3	R15	E3	-33%	+33%

aiming to generate distinct source frames belonging to the corresponding GoS. In this study, 150 source structures are modeled for each of the 3 GoS (resulting in a total of 450 source structures) using the LHS method. The corresponding 21 parameters are varied within a range spanning from 0.25 to 4 times their nominal values. This number of source structures has been chosen to ensure statistically significant results. For each of the 150 structures within a GoS, randomness in the modal properties (i.e., natural frequencies and mode shapes) is simulated on two mechanical parameters ( $E$  and  $\rho$ ), having the highest  $CV_{i,\%}$  from the first sensitivity analysis (Figure 4), resulting in a total of 144 observations per structure. This is feasible because sensitivity analysis effectively identifies the mechanical parameters with the greatest influence on the natural frequencies. To ensure consistency in the target structure, three different analyses are conducted, each involving two varying parameters from the corresponding source GoS. The six selected parameters are presented in Table 6.

## 5. Similarity Analysis of Source to Target Structures

In this section, the results derived from point clouds, representing scaled eigenvector distributions, are used to assess the similarity between source and target structures.

**5.1. Eigenvector Distributions.** The modal characteristics utilized in this study are the natural frequencies and the mode shapes corresponding to the nine DoFs related to the numerical frame model. Each  $k$ -th mode is then scaled by its corresponding natural frequency ( $f_k \Phi_k$ ).

In Figure 6, a point cloud plot of the scaled eigenvector distributions obtained from 144 observations of a single source structure and the target structure is shown. Then, the features are fitted into a Gaussian mixture (GM) model, considering the first three modes for all nine DoFs, with a number of components set to three. This point cloud serves as the basis for computing the  $D_{KL}$  between each source structure and the target structure.

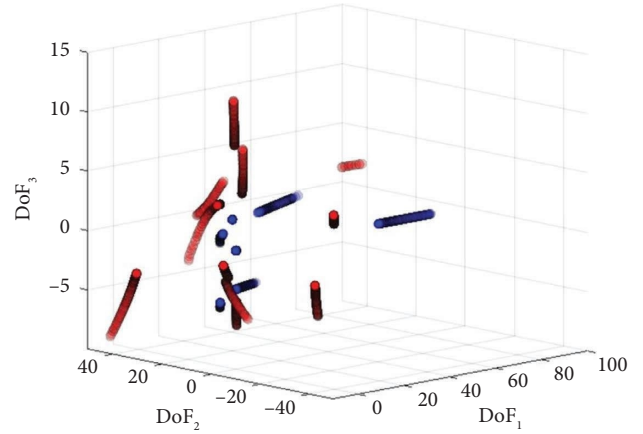


FIGURE 6: Point cloud plot comparing the scaled eigenvector distributions of a single source (red) and target (blue) structure (144 observations). The selected DoFs are the first, second, and third for both structural configurations.

**5.2. Distributions Analysis via GM Models and Kullback-Leibler Divergence.** When the modal properties, such as natural frequencies and mode shapes, are numerically estimated for both target and source structures (belonging to their respective GoS), a distribution analysis can then be performed. Each structure will have a number of observations where mechanical properties modify the stiffness and mass matrices, thereby affecting the outputs of the eigenvalue analysis. Mode shapes are then multiplied for their frequency content. For each  $d$ -th DoF, a structure will have  $m$  scaled mode shapes for each  $n$ -th observation, with these observations varying between two different structures belonging to the same source GoS. The scaled eigenvectors of the target structure, observed  $n$  times, are then compared with those of each source structure from the distinct GoS, using a point cloud plot (Figure 6).

Then, a GM model is defined as a multivariate (multidimensional), multicomponent (equation (14)) version of the classical Gaussian distribution [56], where  $g_i$  is the GM PDF of order  $I$ ,  $\mathbf{x}$  is the multidimensional feature vector  $\mathbb{R}^{dx1}$ ,  $i$  denotes the component, while  $\boldsymbol{\mu}_i$ ,  $\boldsymbol{\Sigma}_i$  and  $w_i$  are the mean vector  $\mathbb{R}^{dx1}$ , covariance matrix  $\mathbb{R}^{dxd}$ , and component proportion  $\mathbb{R}^{1x1}$ , respectively.

$$g_I(\mathbf{x}|\boldsymbol{\mu}_i, \boldsymbol{\Sigma}_i, w_i) = \sum_{i=1}^I w_i (2\pi)^{-(d/2)} |\boldsymbol{\Sigma}_i|^{-(1/2)} \exp\left(-\frac{1}{2}(\mathbf{x} - \boldsymbol{\mu}_i)^T \boldsymbol{\Sigma}_i^{-1} (\mathbf{x} - \boldsymbol{\mu}_i)\right). \quad (14)$$

Considering the divergence of  $q(x)$  from  $p(x)$ , it can be expressed as  $D_{KL}(p(x)||q(x))$ , representing the amount of information lost when  $q(x)$  is used to describe  $p(x)$  [22].

When  $p(x)$  and  $q(x)$  are two probability distributions of the discrete random variable  $x$ , the  $D_{KL}$  formulation is described in the following equation:

$$D_{KL}(p(x)||q(x)) = \sum_{x \in X} p(x) \log_2 \frac{p(x)}{q(x)}. \quad (15)$$

The  $D_{KL}$  is commonly used to measure the “distance” between two probability distributions. However, it is not a true metric, as it does not satisfy the triangle inequality.

Additionally, it is asymmetric, meaning that the  $D_{KL}$  divergence from  $p(x)$  to  $q(x)$  is generally different from that from  $q(x)$  to  $p(x)$ . Nevertheless,  $D_{KL}(p(x)||q(x))$  is a nonnegative measure, meaning that  $D_{KL}(p(x)||q(x)) \geq 0$ , with equality holding if and only if  $p(x) = q(x)$ . The GM model assumes that multidimensional features follow a Gaussian distribution, which is commonly used when the distribution of data is unknown. Even if the data include negative values (Figure 7), the GM model remains mathematically valid, though it may not fully capture the true population distribution. GM models are particularly effective for classifying data when it is symmetrically distributed around the mean, even if they do not perfectly represent the population. This is because GM models are applied consistently to both source and target structures, ensuring that any errors introduced by the model affect both distributions similarly.

When the  $D_{KL}$  reaches a minimum value between the source and target, it suggests an optimal match. However, the discrepancy between datasets cannot be fully eliminated, as the true population distributions are unknown. Thus, the errors introduced by using GM models are inherently accounted for in the  $D_{KL}$  comparison, even though complete elimination of these errors is not possible.

**5.3. Similarity With Respect to Vibration Modes: Comparison to Parameter Deviation.** Initially, it is possible to infer how each source structure differs from the target structure in terms of their parameter values. Each structure (both source and target) will have 144 observations, and the mean values of the parameters are calculated. Then, the mean deviation of the parameters,  $\Delta PAR_{S,h}$ , for each  $h$ -th source structure belonging to the  $S$ -th GoS, is computed according to the following formulation:

$$\Delta PAR_{S,h} = \frac{1}{n_p} \sum_{i=1}^{n_p} \left| \frac{(\overline{SF}_{S,h})_i - (\overline{TF}_T)_i}{(\overline{TF}_T)_i} \right|, \quad (16)$$

where  $\overline{SF}$  and  $\overline{TF}$  represent the mean value of the parameters of the source and target frames, respectively, for the total number of observations (in this work, 144 observations), and  $i$  refers to the parameter, with  $n_p$  representing the total number of parameters. The subscript  $h$  indicates the source structure belonging to the  $S$ -th GoS, while  $T$  is used to specify the target structure, with its randomness in the observations varying according to the corresponding GoS (as per analyses 1, 2, and 3) (Table 6). For each of the 450 source structures, a  $D_{KL}$  value, normalized to the highest one within the corresponding GoS, is determined by analyzing the source and target scaled eigenvectors. Additionally, the corresponding parameters are compared by evaluating their deviation,  $\Delta PAR_{S,h}$ , with respect to the target structure. Figure 8 presents a comparison of the normalized  $D_{KL}$  trends for the source structures across all three GoS. In the figure, each bar plot represents the divergence of a single source structure relative to the target structure. Higher divergence values indicate greater dissimilarity between the structures, while smaller values correspond to more similar

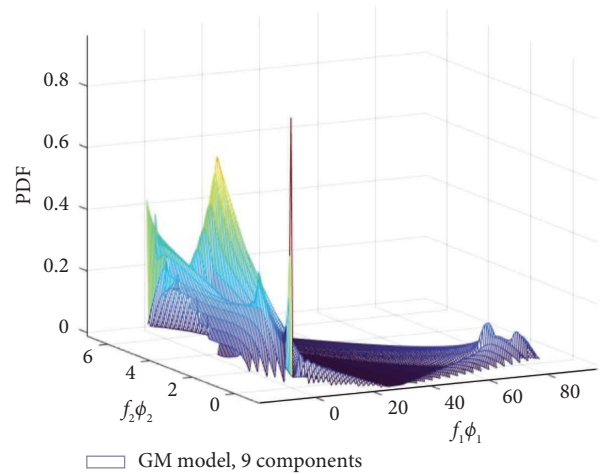


FIGURE 7: GM model representation of the scaled eigenvector distributions of the target structure ( $d=2$  and  $i=9$ ).

structures. This is compared with the mean deviation of parameters,  $\Delta PAR_{S,h}$  (source/target), represented by markers in Figure 8. The trend is almost negligible, consistent with the LHS procedure. It is evident that the same difference in structural properties between two structures does not necessarily result in the same effect in terms of modal properties, that is, natural frequencies and mode shapes. It can be concluded that the normalized  $D_{KL}$  serves as a similarity index for the modal properties of three-story aluminum frames. However, even structures with significant differences, belonging to two distinct GoS, can exhibit similar parameter deviations. In contrast, the divergence measure effectively distinguishes which of the two structures is more similar to the target structure, to achieve the specified objective. Figure 9 presents the flowchart that illustrates the methodology followed in this study.

**5.4. Comparison With Established Similarity Assessment Methods.** Several techniques exist for estimating similarity between structures, depending on the nature of the differences under consideration: topological variations (e.g., addition or removal of structural elements), geometric changes (such as modifications in cross-sectional dimensions), or variations in mechanical parameters (such as Young's modulus and density).

In the case examined in this study, the structural topology remains unchanged: all structures share the same organization in terms of nodes and connections. The variations lie exclusively in the geometrical and mechanical parameters associated with the structural elements. Under these conditions, the well-known Jaccard index [37, 57], commonly used in SHM to compare structures at the topological level, cannot be applied in its classical formulation.

To assess similarity between structures with constant topology but differing physical characteristics, the Gower distance ( $D_{Gower}$ ) [58, 59] was employed. This metric allows for comparison between observations described by heterogeneous variables, whether continuous (e.g., Young's

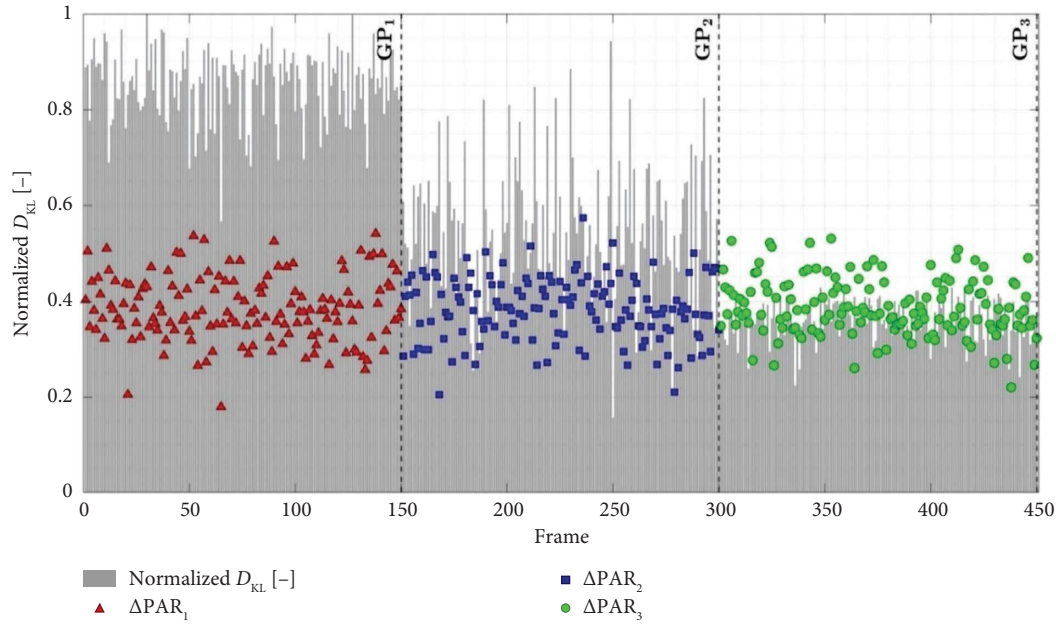


FIGURE 8: Source frames of the corresponding Group of Structures (GoS),  $GP_s$ ; the bar plot represents the normalized Kullback–Leibler divergence ( $D_{KL}$ ) of the scaled eigenvector distributions for each  $h$ -th source structure towards the target structure distribution. The markers represent the mean deviation of parameters,  $\Delta PAR_{S,h}$ , of the  $h$ -th source structure with respect to the target structure. Identical colors correspond to the same GoS ( $GP_s$ ).

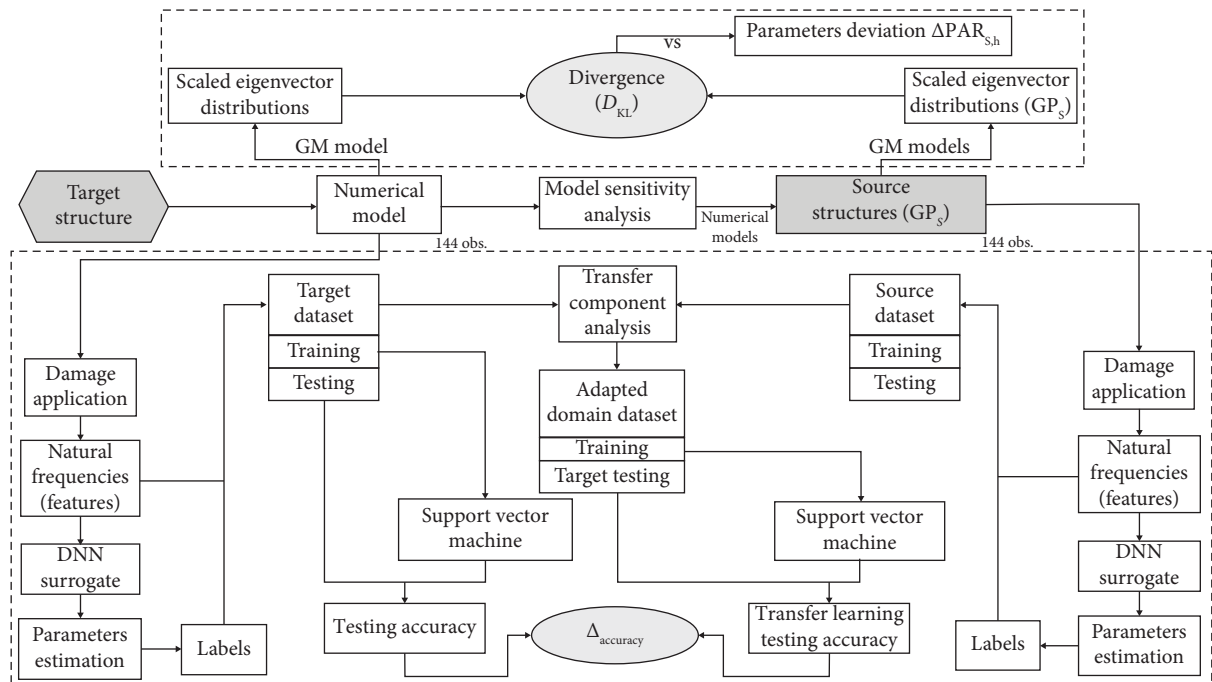


FIGURE 9: Flowchart of the proposed methodology.

modulus), categorical (e.g., material type), or binary.  $D_{Gower}$  yields a value between 0 and 1, where 0 indicates identical observations and 1 denotes maximum dissimilarity. This approach is particularly useful in SHM applications when comparing homologous structures based on geometric and mechanical attributes, especially when the variables are not normalized or of mixed types.

In this context,  $D_{Gower}$  was used as a ground truth reference to evaluate the performance of a proposed similarity index based on modal features, namely the Kullback–Leibler divergence,  $D_{KL}$ . Since  $D_{Gower}$  is independent of modal information, it provides a physically interpretable and topology-invariant baseline for comparison. The results of this analysis are reported in Figure 10.

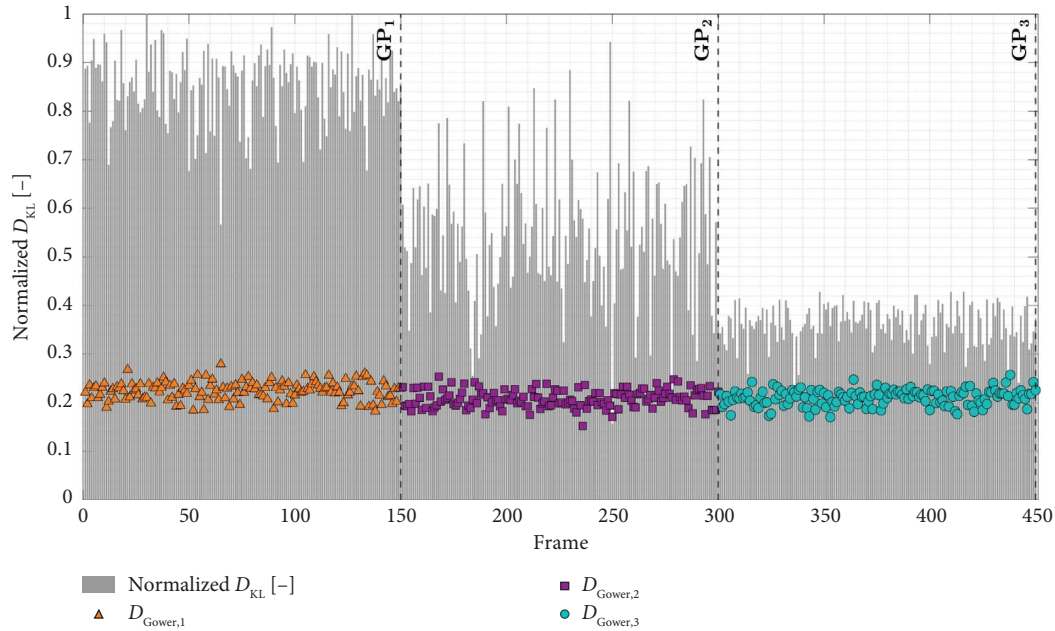


FIGURE 10: Source frames of the corresponding Group of Structures (GoS),  $GP_s$ : the bar plot represents the normalized Kullback–Leibler divergence ( $D_{KL}$ ) of the scaled eigenvector distributions for each  $h$ -th source structure toward the target structure distribution. The markers represent the Gower distance  $D_{Gower,GP_s}$  of the  $h$ -th source structure with respect to the target structure. Identical colors correspond to the same GoS ( $GP_s$ ).

By comparing Figure 8, which shows the similarity estimated via  $D_{KL}$  compared with the scatter between parameters, with the results obtained using  $D_{Gower}$  in Figure 10, it is evident that the two measures yield consistent outcomes. This suggests that the Kullback–Leibler based metric derived from modal information is able to capture structural similarity even in the presence of structures with similar topology, geometry, and mechanical properties.

## 6. Numerical Study on the Influence of Similarity in TL via Surrogate Models

**6.1. Expansion of Damage Cases Using Surrogate Models.** As previously discussed, datasets representing different damaged and undamaged conditions can be extracted. In this section, features and labels of the different classes are gathered for classification analysis, with and without TCA. In detail, within the context of black-box modeling, surrogate models are used to generate numerical representations of even complex numerical models by mapping input data to and output responses. In this study, these models are mainly exploited for the following reasons.

- They invert the numerical models of both source and target structures, introducing a large number of damage conditions for each structure through the LHS method. This procedure allows labeling the structural parameters as “damaged” or “undamaged.” While such data are rarely available in real-world applications, in this case, the use of training data derived from numerical simulations provides a valuable advantage, enhancing the efficiency of the surrogate models.

- In a classification problem, data play a crucial role in developing an effective predictive model. Surrogate models provide the opportunity to expand the range of damage cases starting from the limited training data required for their creation.
- When working with numerical models, the computational time required to extract such datasets can be a limiting factor in research. Surrogate models are known to be much faster than numerical models, such as FE models, for several reasons. One of these is the reduced number of outputs required. In fact, the primary interest typically lies in a few outputs, whereas a numerical model must run entirely, generating arrays or solving partial differential equations (e.g., finite element analysis). Instead, a surrogate model is a tool designed to perform a specific task for which it has been trained for (i.e., a surrogate model can only provide outputs for the natural frequencies it has faced during the training process, and no more).

**6.2. Feedforward Neural Networks Surrogate Models.** Deep neural networks (DNNs) are powerful tools for predicting structural parameters, particularly in addressing complex regression and classification problems [60, 61]. In this context, a fully connected neural network, commonly known as feedforward neural network, is exploited to solve the inverse problem associated with eigenvalue analysis. In this study, natural frequencies are used as input data to develop a surrogate model that can predict the properties of various numerical structures. This approach is expected to optimize the computational effort of numerical models by

avoiding the need for a full-scale analysis whenever only specific results are required. DNN-based surrogate models are used to replace numerical models in introducing damage across many structures, outlining the estimation of parameters belonging to hundreds of different frames using only a natural frequency dataset as input features. The neural network consists of consequent layers of nodes, which describe the mapping of the input–output relationship. The input layer is the first layer of the network, consisting of features (i.e., natural frequencies), with the number of nodes in this layer corresponding to the number of input features. Hidden layers are then used to perform computations on the input data, allowing a learning procedure to extract information through the output layer. The training of a neural network aims to optimize the connections weights and minimize the discrepancies between the actual and predicted output. This optimization process, known as back-propagation, makes use of optimization algorithms to adjust and update the weights based on an error measurement computed during the training process.

In this paper, the Levenberg–Marquardt optimization algorithm [62, 63] is exploited to solve nonlinear least square problems. The output vectors are evaluated as

$$\mathbf{Y}_r = f\left(\sum_{m=1} \mathbf{w}_{rm}^{(0)} \mathbf{H}_m^{(1)} + b_r^{(0)}\right), \quad (17)$$

with  $\mathbf{H}_m^{(1)}$  representing the first hidden layer used to predict output starting from input data  $\mathbf{X}_p$ :

$$\mathbf{H}_m^{(1)} = g\left(\sum_{p=1}^n \mathbf{w}_{mp}^{(1)} \mathbf{X}_p + b_m^{(1)}\right), \quad (18)$$

where the weights parameters are described by  $\mathbf{w}_{rm}^{(0)}$  and  $\mathbf{w}_{mp}^{(1)}$ , and  $b_r^{(0)}$ , while  $b_m^{(1)}$  constitute the bias parameters. In addition,  $f$  and  $g$  describe the activation functions and the error is then computed through the mean squared error (MSE), which measures the average squared difference between the predicted outputs and target values. Then, the Levenberg–Marquardt optimization algorithm is used to minimize the MSE by updating the weights and bias parameters, ultimately reaching an optimal solution.

To extract significant data for DA applications, it is essential to first introduce damages in both the target and source structures. For each of the three damage scenarios, different analyses are conducted. A sampling procedure using LHS is applied, with damages ranging from a minimum value (representing the most severe damage, assumed to be 30% of the undamaged nominal value) to a maximum value, which corresponds to the undamaged nominal value.

It is important to note that the definition of such damage threshold significantly affects the classification performance, particularly near the boundaries of the clusters associated with damaged and undamaged states. As highlighted in [52], thresholds not grounded in structural or statistical knowledge may increase the risk of false alarms in real SHM applications. This study adopts damage levels that reflect a simplified but consistent range of structural degradation,

acknowledging that the reliability of the approach increases with the availability of prior structural knowledge, as highlighted by the *levels of knowledge* concept [64].

To make DA useful, the target/source ratio of the datasets must be small. In this work, this ratio is set to 1/10 (Table 7). Once the natural frequencies are defined, DNN surrogate models are used to estimate the parameter values under damage conditions through regression, starting from the corresponding natural frequencies. Within this, 80% of the dataset has been used for model development and for the actual classification problem, while the remaining 20% is reserved for evaluating the accuracy of the surrogate models (Tables 8 and 9). In particular, for each GoS, three different surrogate models of the corresponding parameter have been trained using feedforward neural networks. These models consist of a first input layer with  $k$ -neurons, with  $k$  equal to the number of features (i.e., natural frequencies) determined from the eigenvalue analysis of the respective sampling case, which reflects a potential damage condition. Then, the hidden layers compute the outputs, updating the weights through an optimization process. The computational properties used in the DNN training procedure are characterized by an Intel(R) Xeon(R) W-2255 CPU @ 3.70 GHz and a 256 GB RAM. Due to different sensitivity of the  $j$ -th applied damage, the architectures of the hidden layers and the corresponding neurons, after a trial-and-error testing procedure, are selected for each parameter estimation and shown in Table 10. The input matrices  $\mathbf{X}_s^l$  for the  $l$ -th surrogate model related to the  $S$ -th GoS are

$$\mathbf{X}_s^l = \left(\mathbf{f}_{1_{h \times j}} \mathbf{f}_{2_{h \times j}} \mathbf{f}_{3_{h \times j}}\right)_s^l, \quad (19)$$

where  $h$  is the source frame considered for the  $j$ -th health state, which could be damaged or undamaged. Following this, after the optimization process of the hidden layer with the input data, the output layer is constituted by a response vector  $\mathbf{Y}_s^l$  of the structural parameter vector  $\mathbf{p}$  as follows:

$$\mathbf{Y}_s^l = \left(\mathbf{p}_{h \times j}\right)_s^l, \quad (20)$$

which has dimension  $h \times j$ . The datasets are portioned into training, validation, and testing sets, representing 70%, 15%, and 15% of the total data, respectively. The performance is then evaluated using the MSE, and the final correlations  $R$  between predicted and target values are computed for each model.

**6.3. Estimated Parameters for Labeling Purposes via Surrogate Models.** For classification purposes, labels are of relevant importance. Here, the MSE error and the correlation  $R$  are reported for a DNN model [65], aimed at predicting the mechanical parameter (material density  $\rho$ ) associated with the first damage scenario considered (Figure 11). Subsequently, 20% of the original dataset is used as novel input data for the corresponding surrogate model. Table 8 presents the parameter testing accuracies of the target system for the related analysis, evaluated with a tolerance of 3%. Each analysis is conducted by generating input data based on the

TABLE 7: Dataset subdivisions for DNN surrogate models.

DNN dataset	Source #	Target #
Total dataset for a single structure subjected to damage 1, 2, or 3	2000	200
Model training dataset [80%]	1600	160
Testing dataset (to be used for DA) [20%]	400	40

TABLE 8: Accuracy of the DNN surrogate models of the target structure for the related analysis.

Damage	Analysis 1 (%)	Analysis 2 (%)	Analysis 3 (%)
R17	100	100	100
H10	100	100	100
A14	100	100	100

TABLE 9: Accuracy of the DNN surrogate models of the source structures belonging to their Group of Structures (GoS),  $GP_S$ .

Damage	$GP_1$ (%)	$GP_2$ (%)	$GP_3$ (%)
R17	98.85	99.70	99.68
H10	99.89	99.07	99.92
A14	99.99	99.95	99.75

TABLE 10: Deep neural network (DNN) surrogate model layer architecture description.

Surrogate model	7-Hidden layers architecture (neurons)
$DNN_{R17}$	[10 30 50 70 50 30 10]
$DNN_{H10}$	[10 30 50 70 50 30 10]
$DNN_{A14}$	[10 30 50 70 50 30 10]

varying parameters listed in Table 6, while Table 8 shows the corresponding accuracies for the source systems within each GoS.

#### 6.4. Multiclass Damage Detection on the Target Structure.

Once damages have been applied to the target structure and the related labels are defined, a classification analysis for damage detection can be performed using SVM, with 75% of the data used for training and 25% for testing. To train the SVM model, labels corresponding to both the undamaged and damaged conditions must be considered. Therefore, it is assumed that these labels are available for the target structure during the training phase. The accuracies of the three target structures, obtained through the varying parameters listed in Table 6, are highlighted (Table 11). Damage detection results are then presented by considering the accuracy related to each class. A confusion (or error) matrix [66] is used to show the comparison (in terms of accuracy) between the true class associated with a specific damaged or undamaged condition (ground truth) and the predicted class identified by the algorithm. Figure 12 shows the confusion matrix related to the damaged and undamaged conditions for each analysis.

**6.5. TCA Results.** TCA can be performed by considering all possible datasets of source structures related to the different GoS. Then, on the adapted domain, the testing data from the

testing structures are classified, and the corresponding accuracies relative to the actual labels are extracted. To obtain significant results, the mean accuracies, determined by adapting the datasets of the 150 source structures describing a GoS, are discussed (Table 11). Figure 13 shows the related confusion matrices for the damaged/undamaged conditions of the target testing data, and the related accuracy of the classification model is shown in Table 12.

**6.6. Impact of Vibration Modes Similarity on TL.** Finally, as previously described, two different results are obtained by comparing the accuracies for the target testing data: first, by conducting a classification analysis on the original datasets, and second, on the adapted domains.

The mean algebraic difference between the prediction results with and without the use of TCA (mean  $\Delta_{\text{accuracy}}$ ) can now be computed for each analysis related to the source structures linked to the group of similarity GoS under consideration.

This highlights the relationship between similarity, as indicated by scaled eigenvector distributions (using the mean  $D_{KL}$  results within the same GoS) and the accuracy improvements achieved through TCA. These analyses are performed for each mean accuracy value obtained from the 150 datasets of the corresponding GoS, as shown in Figure 14.

As observed, there is a trend where the benefits of TCA on the target domain increase when the source datasets originate from structures characterized by more similar behavior in terms of vibration modes, as confirmed by the normalized  $D_{KL}$ .

Furthermore, this trend remains consistent regardless of the actual distance in properties between the source and target structures.

Thus, *negative transfer* can be mitigated when the source structure selected for DA exhibits greater similarity in vibration modes, independent of direct geometric and mechanical similarities.

#### 6.7. General Considerations on the Correct Choice of Source Structures.

It is now possible to outline general criteria for selecting the most suitable source structures. While numerical models have been used to generate features thus far, in many real-world scenarios, the primary challenge lies in the limited experimental data available for the target structure, coupled with a lack of associated knowledge. In the following, the same three-story topological frames are considered to select the appropriate source data, by varying the properties of the main structural elements. In the analyses performed (Figure 14), it is evident that the group of source structures GoS more dissimilar to the target structure

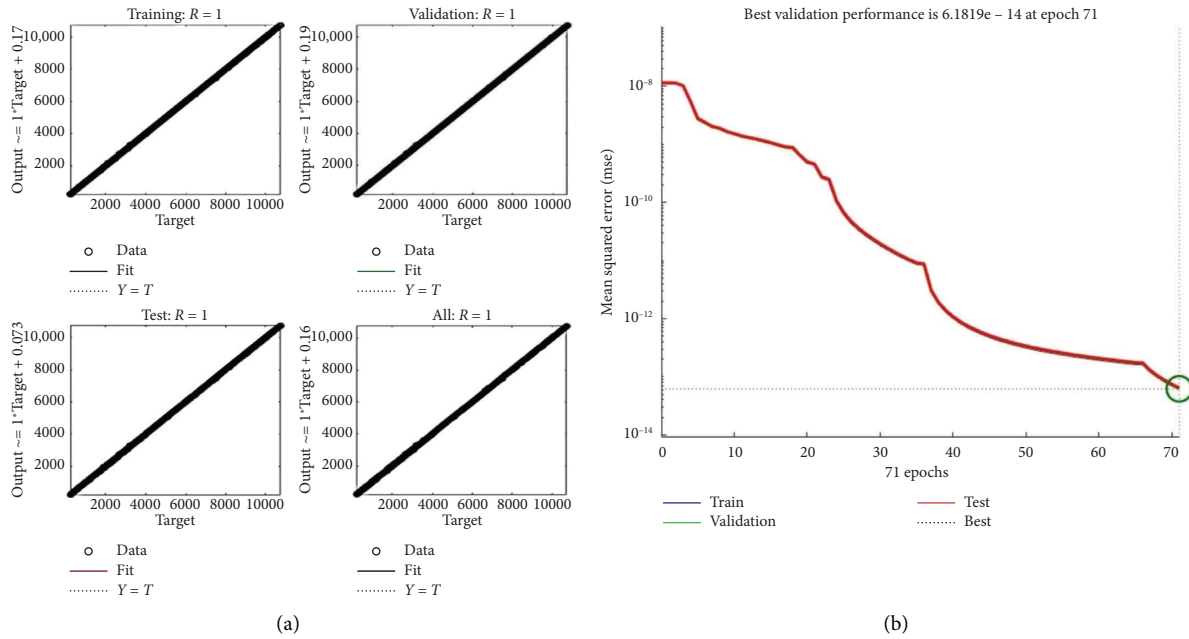


FIGURE 11: Regression plot for the training, validation, and testing of the DNN surrogate model related to damage in the material density (R17) (a). Convergence (MSE) of the DNN surrogate model for damage introduction in the material density (R17) (b).

TABLE 11: Testing accuracy of the classification model for the target structure original domains belonging to the analysis considered.

Target structure	Analysis 1 (%)	Analysis 2 (%)	Analysis 3 (%)
Test accuracy (SVM)	90.00	76.67	80.00

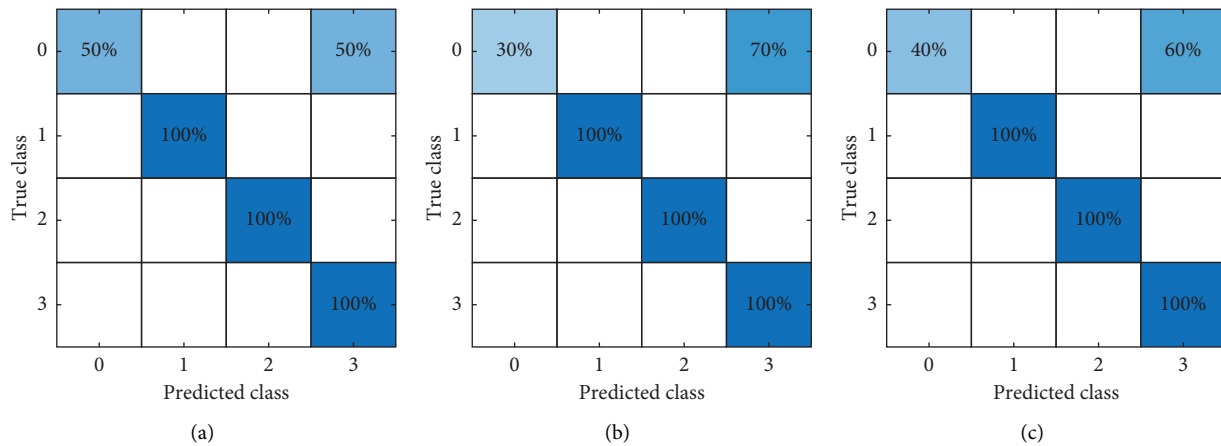


FIGURE 12: Confusion matrices for the target testing original dataset across the three different analyses (class 0 represents the undamaged condition, class 1 is related to damage 1 (R17), class 2 to damage 2 (H10), while class 3 corresponds to damage 3 (A14). White cells represent no prediction). First target analysis (a); second target analysis (b); and third target analysis (c).

(GP<sub>1</sub>) shows the lowest performance in damage detection accuracy (+0.00%). Furthermore, negative transfer could have occurred when transferring features from this group, making it the most unsuitable case. The second GoS (GP<sub>2</sub>), which has a mean divergence in the middle range, yielded modest results (+1.38%). Lastly, the highest performance is appreciated for the most similar GoS (GP<sub>3</sub>), achieving a significant accuracy increment (+10.80%), which is highly relevant in this type of application.

Modal properties have proven to be useful parameters for detecting similarity through divergence measures. The higher the divergence, the less suitable the selected source dataset is for DA. Therefore, once modal parameters from a set of known structures are obtained, the source dataset can be selected by comparing the divergence outputs and choosing the datasets with the minimum value among all possible choices. However, this does not always prevent negative transfer if all the source structures are unsuitable for the problem.

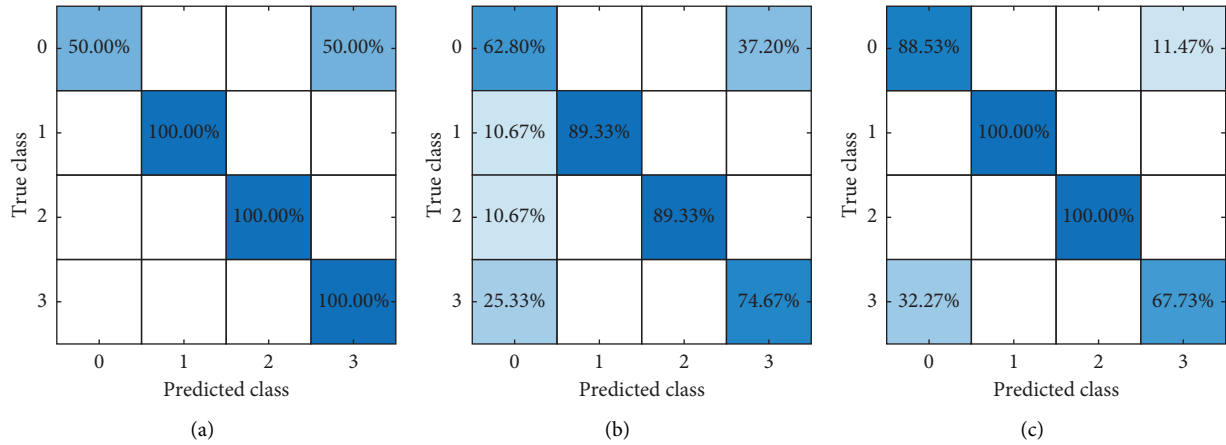


FIGURE 13: Confusion matrices of the target testing adapted dataset across the three different analyses (class 0 represents the undamaged condition, class 1 is related to the damage 1 (R17), class 2 to damage 2 (H10), while class 3 corresponds to damage 3 (A14)). First adapted domain target analysis (a); second adapted domain target analysis (b); and third adapted domain target analysis (c).

TABLE 12: Testing accuracy of the classification model for the target structure adapted domains belonging to the analysis considered.

Target structure	Analysis 1 (%)	Analysis 2 (%)	Analysis 3 (%)
Mean test accuracy (TCA)	90.00	78.04	90.80

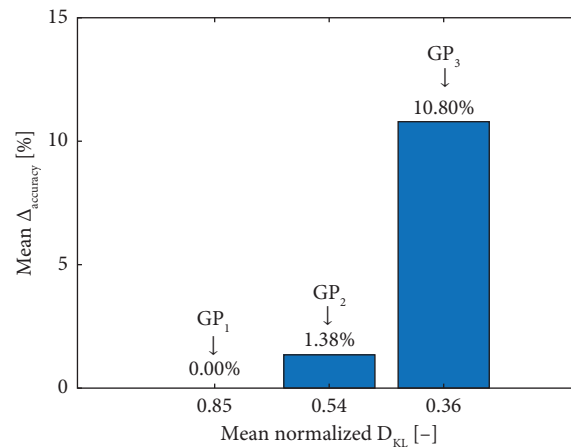


FIGURE 14: Plot representing the similarity within the scaled eigenvector distributions on the  $x$ -axis (measured by the mean normalized  $D_{KL}$ ) versus the mean difference in accuracy for the testing classification problem of target structure, with and without TCA ( $y$ -axis). The corresponding Group of Structures (GoS), GP<sub>S</sub>, is highlighted as well (GP<sub>1</sub>-GP<sub>2</sub>-GP<sub>3</sub>).

A general procedure can be outlined as follows. First, the source structures that provide modal parameters, which are used as features, must be selected. Once the target features are obtained, the divergence between the source and target data distributions is computed. The source structure exhibiting the lowest divergence value is then chosen, as it demonstrates the greatest similarity to the target structure. Finally, DA can be applied within the selected source and target domains by performing a classification procedure, with labels available during the model training process for both source and target structures, to identify anomalies in the structural health state of the target structure.

## 7. Conclusions

In this paper, an innovative approach for assessing similarity in DA for structural health monitoring is proposed. When dealing with dynamically monitored structures, it is challenging to determine a priori which data are most suitable for knowledge transfer. This work addressed this open question by exploring similarity in geometric, mechanical, and topological perspectives with the context of population-based structural health monitoring.

In this study, the authors demonstrate that Kullback-Leibler divergence measures of modal distributions are an

effective tool for selecting the optimal pair of source and target structure in DA, when performing multiclass damage detection.

A three-story aluminum frame has been considered in this paper, and a modal sensitivity analysis has been performed to define the source structures based on their parameters. Mode shapes distributions, scaled by their corresponding natural frequencies, are used to calculate the Kullback–Leibler divergence for each source structure relative to the target structure. The results show that distributions from structures generated by varying more sensitive parameters exhibit higher divergence compared to those generated by varying less sensitive parameters, while maintaining a constant parameters distance for all structures. By applying DA, datasets from source structures with higher similarity to the target structure yield greater improvements in damage classification accuracy.

The main conclusions of the work are outlined hereinafter:

- Even when dynamic data are considered, structures that are highly dissimilar in terms of topology, geometry, and mechanical quantities can still exhibit similarity for DA applications.
- A *similarity index* based on the normalized Kullback–Leibler divergence of modal features is proposed and validated for DA applications. The proposed *similarity index* outperforms other similarity distances based on topology, geometry, and mechanical quantities.

As a future perspective, the proposed *similarity index* will be applied to design dynamic sensing systems optimized to receive information from one (or more) already highly equipped structures and to identify source equipped structures that are less prone to negative transfer.

### Data Availability Statement

The data that support the findings of this study are available from the corresponding author upon reasonable request.

### Conflicts of Interest

The authors declare no conflicts of interest.

### Funding

This research was supported by project PNRR-NGEU, which has received funding from the MUR–DM 118/2023, and Next Generation EU Within the PRIN 2022 PNRR Program, Grant/Award number: D.D.1409, 14/09/2022 MIUR.

### Acknowledgments

This publication is part of the project PNRR-NGEU, which has received funding from the MUR–DM 118/2023. This study was carried out within the «SAT4SHM» project—funded by European Union—Next Generation EU within the PRIN 2022 PNRR program (D.D.1409, 14/09/2022 MIUR).

### References

- [1] C. Farrar and K. Worden, “Structural Health Monitoring A Machine Learning Perspective,” *Structural Health Monitoring: A Machine Learning Perspective* (2012): <https://doi.org/10.1002/9781118443118>.
- [2] R. Ceravolo, “Structural and seismic monitoring of historical and contemporary buildings: general principles and applications,” *Memorie Della Accademia Delle Scienze di Torino*, 2 (Classe di Scienze Fisiche Matematiche E Naturali, VI Serie, 2023).
- [3] G. Coletta, G. Miraglia, P. Gardner, R. Ceravolo, C. Surace, and K. Worden, “A Transfer Learning Application to FEM and Monitoring Data for Supporting the Classification of Structural Condition States,” in *European Workshop on Structural Health Monitoring*, ed. P. Rizzo and A. Milazzo (Cham: Springer International Publishing, 2021), 947–957.
- [4] K. Smarsly, K. Dragos, and J. Wiggenbrock, “Machine Learning Techniques for Structural Health Monitoring” (2016).
- [5] K. Worden and G. Manson, “The Application of Machine Learning to Structural Health Monitoring,” *Philosophical Transactions of the Royal Society A: Mathematical, Physical and Engineering Sciences* 365, no. 1851 (2006): 515–537, <https://doi.org/10.1098/rsta.2006.1938>.
- [6] G. Coletta, “Monitoring of Architectural Heritage With Machine Learning Methods,” (2022), <https://iris.polito.it/handle/11583/29711171-235>.
- [7] J.-J. Sinou, “A Review of Damage Detection and Health Monitoring of Mechanical Systems From Changes in the Measurement of Linear and Non-Linear Vibrations,” *Mechanical vibrations: Measurement, Effects and Control* (2009): 643–702.
- [8] W. Fan and P. Qiao, “Vibration-Based Damage Identification Methods: A Review and Comparative Study,” *Structural Health Monitoring* 10 (2011): 83–111.
- [9] R. Ditommaso, M. Mucciarelli, and F. C. Ponzio, “Analysis of Non-Stationary Structural Systems by Using a Band-Variable Filter,” *Bulletin of Earthquake Engineering* 10, no. 3 (2012): 895–911, <https://doi.org/10.1007/s10518-012-9338-y>.
- [10] R. Ceravolo, “Time-Frequency Analysis,” *Chapter 26 in Encyclopedia of Structural Health Monitoring*, Boller, Chang and Fujino (Wiley & Sons Ltd, 2009).
- [11] P. Gardner, X. Liu, and K. Worden, “On the Application of Domain Adaptation in Structural Health Monitoring,” *Mechanical Systems and Signal Processing* 138 (2020): 106550, <https://doi.org/10.1016/j.ymsp.2019.106550>.
- [12] W. Dai, Q. Yang, G. R. Xue, and Y. Yu, “Boosting for Transfer Learning,” in *Proceeding 24th International Conference on Machine Learning* (2007), 193–200, <https://doi.org/10.1145/1273496.1273521>.
- [13] S. J. Pan and Q. Yang, “A Survey on Transfer Learning,” *IEEE Transactions on Knowledge and Data Engineering* 22, no. 10 (2010): 1345–1359, <https://doi.org/10.1109/tkde.2009.191>.
- [14] M. E. Taylor and P. Stone, “Transfer Learning for Reinforcement Learning Domains: A Survey,” *Journal of Machine Learning Research* 10, no. 1 (2009): 1633–1685.
- [15] K. Weiss, T. M. Khoshgoftaar, and D. D. Wang, “A Survey of Transfer Learning,” *Journal of Big Data* 3, no. 1 (2016): 9, <https://doi.org/10.1186/s40537-016-0043-6>.
- [16] C. Xiangyu, C. Liang, C. Jianyun, et al., “Unsupervised Domain Adaptation Damage Identification Approach of High Arch Dams After Earthquakes,” *Structural Control and Health*

- Monitoring* 2023 (2023): 1–18, <https://doi.org/10.1155/2023/6349167>.
- [17] K. Dunphy, A. Sadhu, and J. Wang, “Multiclass Damage Detection in Concrete Structures Using a Transfer Learning-Based Generative Adversarial Networks,” *Structural Control and Health Monitoring* 29, no. 11 (2022): <https://doi.org/10.1002/stc.3079>.
- [18] N. Bao, T. Zhang, R. Huang, S. Biswal, J. Su, and Y. Wang, “A Deep Transfer Learning Network for Structural Condition Identification With Limited Real-World Training Data,” *Structural Control and Health Monitoring* 2023 (2023): 1–18, <https://doi.org/10.1155/2023/8899806>.
- [19] L. Wu, X. Lin, Z. Chen, P. Lin, and S. Cheng, “Surface Crack Detection Based on Image Stitching and Transfer Learning With Pretrained Convolutional Neural Network,” *Structural Control and Health Monitoring* 28, no. 8 (2021): <https://doi.org/10.1002/stc.2766>.
- [20] S.-Y. Chen, Y.-W. Wang, Y.-Q. Ni, and Y. Zhang, “When Transfer Learning Meets Dictionary Learning: A New Hybrid Method for Fast and Automatic Detection of Cracks on Concrete Surfaces,” *Structural Control and Health Monitoring* 2024, no. 1 (2024): 3185640, <https://doi.org/10.1155/2024/3185640>.
- [21] L. A. Bull, P. A. Gardner, J. Gosliga, et al., “Foundations of Population-Based SHM, Part I: Homogeneous Populations and Forms,” *Mechanical Systems and Signal Processing* 148 (2021): 107141, <https://doi.org/10.1016/j.ymssp.2020.107141>.
- [22] S. Kullback and R. A. Leibler, “On Information and Sufficiency,” *The Annals of Mathematical Statistics* 22, no. 1 (1951): 79–86, <https://doi.org/10.1214/aoms/1177729694>.
- [23] P. Gardner, L. A. Bull, J. Gosliga, N. Dervilis, and K. Worden, “Foundations of Population-Based SHM, Part III: Heterogeneous Populations-Mapping and Transfer,” *Mechanical Systems and Signal Processing* 149 (2021): 107142, <https://doi.org/10.1016/j.ymssp.2020.107142>.
- [24] C. T. Wickramarachchi, E. Maguire, E. J. Cross, and K. Worden, “Measuring Data Similarity in Population-Based Structural Health Monitoring Using Distance Metrics,” *Structural Health Monitoring* 23, no. 4 (2023): 2609–2635, <https://doi.org/10.1177/14759217231207526>.
- [25] S.-H. Cha, “Comprehensive Survey on Distance/Similarity Measures between Probability Density Functions,” *International Journal of Mathematical Models and Methods in Applied Sciences* 1 (2007): 300–307.
- [26] T. Kailath, “The Divergence and Bhattacharyya Distance Measures in Signal Selection,” *IEEE Transactions on Communications* 15, no. 1 (1967): 52–60, <https://doi.org/10.1109/tcom.1967.1089532>.
- [27] S. M. Ali and S. D. Silvey, “A General Class of Coefficients of Divergence of One Distribution From Another,” *Journal of the Royal Statistical Society-Series B: Statistical Methodology* 28, no. 1 (1966): 131–142, <https://doi.org/10.1111/j.2517-6161.1966.tb00626.x>.
- [28] I. Csiszár, “Information-Type Measures of Difference of Probability Distributions and Indirect Observations,” *Studia Scientiarum Mathematicarum Hungarica* 2 (1967): 299–318.
- [29] M. Basseville, “Divergence Measures for Statistical Data Processing—An Annotated Bibliography,” *Signal Processing* 93, no. 4 (2013): 621–633, <https://doi.org/10.1016/j.sigpro.2012.09.003>.
- [30] I. Vajda, *Theory of Statistical Inference and Information* (Kluwer Academic Publishers, 1989).
- [31] F. Liese and I. Vajda, “On Divergences and Informations in Statistics and Information Theory,” *IEEE Transactions on Information Theory* 52, no. 10 (2006): 4394–4412, <https://doi.org/10.1109/tit.2006.881731>.
- [32] B. K. Sriperumbudur, K. Fukumizu, A. Gretton, B. Schölkopf, and G. R. G. Lanckriet, “On Integral Probability Metrics,  $\phi$ -Divergences and Binary Classification” (2009).
- [33] A. Müller, “Integral Probability Metrics and Their Generating Classes of Functions,” *Advances in Applied Probability* 29, no. 2 (1997): 429–443, <https://doi.org/10.2307/1428011>.
- [34] M. Pastor, M. Binda, and T. Harčarik, “Modal Assurance Criterion,” *Procedia Engineering* 48 (2012): 543–548, <https://doi.org/10.1016/j.proeng.2012.09.551>.
- [35] A. J. Hughes, J. Poole, N. Dervilis, P. Gardner, and K. Worden, “Quantifying the Value of Information Transfer in Population-Based SHM” (2023).
- [36] A. Bunce, D. S. Brennan, A. Ferguson, et al., “On Population-Based Structural Health Monitoring for Bridges: Comparing Similarity Metrics and Dynamic Responses Between Sets of Bridges,” *Mechanical Systems and Signal Processing* 216 (2024): 111501, <https://doi.org/10.1016/j.ymssp.2024.111501>.
- [37] J. Gosliga, P. A. Gardner, L. A. Bull, N. Dervilis, and K. Worden, “Foundations of Population-Based SHM, Part II: Heterogeneous Populations-Graphs, Networks, and Communities,” *Mechanical Systems and Signal Processing* 148 (2021): 107144, <https://doi.org/10.1016/j.ymssp.2020.107144>.
- [38] G. Delo, C. Surace, K. Worden, and D. S. Brennan, “On the Influence of Structural Attributes for Assessing Similarity in Population-Based Structural Health Monitoring” (2023).
- [39] E. M. Tronci, H. Beigi, M. Q. Feng, and R. Betti, “Transfer Learning from Audio Domains a Valuable Tool for Structural Health Monitoring,” in *Dynamics of Civil Structures*, ed. K. Grimmelmann, 2 (Cham: Springer International Publishing, 2025), 99–107, [https://doi.org/10.1007/978-3-030-77143-0\\_11](https://doi.org/10.1007/978-3-030-77143-0_11).
- [40] V. Cavanni, R. Ceravolo, and G. Miraglia, “A Domain Adaptation Methodology for Enhancing the Classification of Structural Condition States in Continuously Monitored Historical Domes,” *Computer-Aided Civil and Infrastructure Engineering* 39, no. 24 (2024): 3721–3740, <https://doi.org/10.1111/mice.13313>.
- [41] M. Gönen and A. Margolin, “Kernelized Bayesian Transfer Learning,” in *Proceedings of the AAAI Conference on Artificial Intelligence* (2014), <https://doi.org/10.1609/aaai.v28i1.8948>.
- [42] J. Poole, P. Gardner, N. Dervilis, L. Bull, and K. Worden, “On Statistic Alignment for Domain Adaptation in Structural Health Monitoring,” *Structural Health Monitoring* 22, no. 3 (2022): 1581–1600, <https://doi.org/10.1177/14759217221110441>.
- [43] J. Maeck and G. De Roeck, “Description of Z24 Benchmark,” *Mechanical Systems and Signal Processing* 17, no. 1 (2003): 127–131, <https://doi.org/10.1006/mssp.2002.1548>.
- [44] K. Maes and G. Lombaert, “Monitoring Railway Bridge KW51 Before, During, and After Retrofitting,” *Journal of Bridge Engineering* 26, no. 3 (2021): 04721001, [https://doi.org/10.1061/\(asce\)be.1943-5592.0001668](https://doi.org/10.1061/(asce)be.1943-5592.0001668).
- [45] V. Giglioni, J. Poole, I. Venanzi, F. Ubertini, and K. Worden, “A Domain Adaptation Approach to Damage Classification With an Application to Bridge Monitoring,” *Mechanical Systems and Signal Processing* 209 (2024): 111135, <https://doi.org/10.1016/j.ymssp.2024.111135>.
- [46] P. Gardner, L. A. Bull, N. Dervilis, and K. Worden, “Overcoming the Problem of Repair in Structural Health Monitoring: Metric-Informed Transfer Learning,” *Journal of Sound and Vibration* 510 (2021): 116245, <https://doi.org/10.1016/j.jsv.2021.116245>.

- [47] S. J. Pan, I. W. Tsang, J. T. Kwok, and Q. Yang, "Domain Adaptation via Transfer Component Analysis," *IEEE Transactions on Neural Networks* 22, no. 2 (2011): 199–210, <https://doi.org/10.1109/tnn.2010.2091281>.
- [48] B. Schölkopf, A. Smola, and K. R. Müller, "Nonlinear Component Analysis as a Kernel Eigenvalue Problem," *Neural Computation* 10, no. 5 (1998): 1299–1319, <https://doi.org/10.1162/089976698300017467>.
- [49] A. Saltelli, K. Chan, and E. M. Scott, "Sensitivity Analysis" (2000).
- [50] H. Sohn, "Effects of Environmental and Operational Variability on Structural Health Monitoring," *Philosophical Transactions of the Royal Society A: Mathematical, Physical and Engineering Sciences* 365, no. 1851 (2007): 539–560, <https://doi.org/10.1098/rsta.2006.1935>.
- [51] R. Ceravolo, E. Matta, A. Quattrone, and L. Zanotti Fragonara, "Amplitude Dependence of Equivalent Modal Parameters in Monitored Buildings During Earthquake Swarms," *Earthquake Engineering & Structural Dynamics* 46, no. 14 (2017): 2399–2417, <https://doi.org/10.1002/eqe.2910>.
- [52] R. Ditommaso and F. C. Ponzo, "Identifying Damage in Structures: Definition of Thresholds to Minimize False Alarms in SHM Systems," *Buildings* 14, no. 3 (2024): 821, <https://doi.org/10.3390/buildings14030821>.
- [53] M. Stein, "Large Sample Properties of Simulations Using Latin Hypercube Sampling," *Technometrics* 29, no. 2 (1987): 143–151, <https://doi.org/10.2307/1269769>.
- [54] D. E. Huntington and C. S. Lyrintzis, "Improvements to and Limitations of Latin Hypercube Sampling," *Probabilistic Engineering Mechanics* 13, no. 4 (1998): 245–253, [https://doi.org/10.1016/s0266-8920\(97\)00013-1](https://doi.org/10.1016/s0266-8920(97)00013-1).
- [55] R. Ferrari, D. Froio, E. Rizzi, C. Gentile, and E. Chatzi, "Model Updating of a Historic Concrete Bridge by Sensitivity- and Global Optimization-Based Latin Hypercube Sampling," *Engineering Structures* 179 (2019): 139–160, <https://doi.org/10.1016/j.engstruct.2018.08.004>.
- [56] G. J. McLachlan, S. X. Lee, and S. I. Rathnayake, "Finite Mixture Models," *Annual Review of Statistics and Its Application* 6, no. 1 (2019): 355–378, <https://doi.org/10.1146/annurev-statistics-031017-100325>.
- [57] P. Jaccard, "Etude de la Distribution Florale Dans Une Portion Des Alpes et du Jura," *Bulletin de la Societe Vaudoise des Sciences Naturelles* 37 (1901): 547–579.
- [58] J. C. Gower, "A General Coefficient of Similarity and Some of Its Properties," *Biometrics* 27, no. 4 (1971): 857–871, <https://doi.org/10.2307/2528823>.
- [59] K. Agustin, H. Soewandi, and S. Widjojo, "On the Weights for Characteristics and Comparables for Property Valuation Using Quality Rating Valuation Estimation," *Civil Engineering Dimension* 25, no. 1 (2023): 37–47, <https://doi.org/10.9744/ced.25.1.37-47>.
- [60] I. Goodfellow, Y. Bengio, and A. Courville, *Deep Learning* (MIT Press, 2016).
- [61] M. Minsky and S. A. Papert, "Perceptrons: An Introduction to Computational Geometry" (2017), <https://doi.org/10.7551/mitpress/11301.001.0001>.
- [62] K. Levenberg, "A Method for the Solution of Certain Non-Linear Problems in Least Squares," *Quarterly of Applied Mathematics* 2, no. 2 (1944): 164–168, <https://doi.org/10.1090/qam/10666>.
- [63] D. Marquardt, "An Algorithm for Least-Squares Estimation of Nonlinear Parameters," *Journal of the Society for Industrial and Applied Mathematics* 11, no. 2 (1963): 431–441, <https://doi.org/10.1137/0111030>.
- [64] International Scientific Committee on the Analysis and Restoration of Structures of Architectural Heritage (ISCARSAH), "Guidelines for the Analysis, Conservation and Structural Restoration of Architectural Heritage" (2024).
- [65] M. Beale, M. Hagan, and H. Demuth, *Matlab Deep Learning Toolbox Users Guide: Pdf Documentation for Release R2022b* (The MathWorks, Inc, 2022).
- [66] R. G. Congalton, O. Richard, and R. A. Mead, "Assessing Landsat Classification Accuracy Using Discrete Multivariate Analysis Statistical Techniques," *Photogrammetric Engineering & Remote Sensing* (1983): 1671–1678.